Journal of Medicinal Chemistry

Article

Highly potent and selective ecto-nucleotide pyrophosphatase/ phosphodiesterase I inhibitors based on an adenosine 5'-(# or #) thio, (#,#- or #,#)-methylene triphosphate scaffold

Yael Nadel, Joanna Lecka, Yocheved Gilad, Gal Ben-David, Daniel Förster, Georg Reiser, Sarah Kenigsberg, Jean Camden, Gary A Weisman, Hanoch Senderowitz, Jean Sévigny, and Bilha Fischer

J. Med. Chem., **Just Accepted Manuscript** • DOI: 10.1021/jm500196c • Publication Date (Web): 20 May 2014

Highly potent and selective ecto-nucleotide pyrophosphatase/phosphodiesterase I inhibitors based on an adenosine 5'- (α or γ) thio, (α,β- or β,γ)-methylene triphosphate scaffold

Yael Nadel[a§], Joanna Lecka[b,c§], Yocheved Gliad[a], Gal Ben-David[a], Daniel Förster[d], Georg Reiser[d], Sarah Kenigsberg,[a] Jean Camden[e], Gary A. Weisman[e], Hanoch Senderowitz[a]*, Jean Sévigny,[b,c]* and Bilha Fischer[a]*

[a] Department of Chemistry, Bar-Ilan University, Ramat-Gan 52900 Israel,

[b] Département de microbiologie-infectiologie et d'immunologie, Faculté de Médecine, Université Laval, Québec, QC, Canada.

[c] Centre de recherche du CHU de Québec, Québec, QC, Canada.

[d] Otto von Guericke University, Leipziger Str. 44, 39120, Magdeburg, Germany

[e] Biochemistry Department, 540E Bond Life Sciences Center, University of Missouri Columbia, Columbia, Missouri 65211

[*§]These authors contributed equally to this work

*Address correspondence to either co-senior author:

Bilha Fischer

Department of Chemistry, Bar-Ilan University

Ramat-Gan 52900, Israel

Fax: 972-3-6353907; tel.: 972-3-5318303

e-mail: bfischer@mail.biu.ac.il

Jean Sévigny

Centre de Recherche du CHU de Québec

2705 Laurier Blvd., Room T1-39

Québec, QC, Canada G1V 4G2

Fax: 418-654-2765; tel.: 418-654-2772

Email: Jean.Sevigny@crchul.ulaval.ca

Hanoch Senderowitz

Department of Chemistry, Bar-Ilan University

Ramat-Gan 52900, Israel

Fax: 972-3-7384588; tel.: 972-3-7384588

e-mail: hsenderowitz@gmail.com

Abbreviations: $[Ca^{2+}]_i$, intracellular Ca^{2+} concentration; CDI, carbonyldimidazole; NPP, ecto-nucleotide pyrophosphatase/phosphodiesterase; NTPDase, ecto-nucleoside triphosphate diphosphohydrolase; ESI, electron spray ionization; HRMS-MALDI, high-resolution mass spectrometry matrix-assisted laser desorption ionization; P2R, P2 receptor; NTP, nucleoside–5'-triphosphate; pNP-TMP, thymidine 5'-monophosphate p-nitrophenyl ester; RT, room temperature; SD, standard deviation; TEAA,

triethylammonium acetate; TEAB, triethylammonium bicarbonate; CPPD, calcium pyrophosphate dihydrate; GFP, green fluorescent protein; hERG, human Ether-à-go-go-Related Gene; PDB, protein database.

Abstract

Aberrant nucleotide pyrophosphatase/phosphodiesterase-1 (NPP1) activity is associated with chondrocalcinosis, osteoarthritis, and type 2 diabetes. The potential of NPP1 inhibitors as therapeutic agents, and the scarceness of their structure-activity relationship, encouraged us to develop new NPP1 inhibitors. Specifically, we synthesized ATP-α-thio-β,γ-CH_2 (**1**), ATP-α-thio-β,γ-CCl_2 (**2**), ATP-α-CH_2-γ-thio (**3**), and 8-SH-ATP (**4**), and established their resistance to hydrolysis by NPP1,-3 and NTPDase1,-2,-3 and -8 (<5% hydrolysis). Analogues **1-3** at 100 μM inhibited pNP-TMP hydrolysis by NPP1 and NPP3 by > 90% and 23-43%, respectively, and only slightly affected (0-40%) hydrolysis of ATP by NTPDase1,-2,-3,-8. Analogue **3** is the most potent NPP1 inhibitor currently known, K_i 20 nM and IC_{50} 0.39 μM. Analogue **2a** is a selective NPP1 inhibitor with K_i 685 nM and IC_{50} 0.57 μM. Analogues **1-3** were found mostly to be non-agonists of $P2Y_1$/$P2Y_2$/$P2Y_{11}$ receptors. Docking analogues **1-3** into NPP1 model suggested that activity correlates with the number of H-bonds with binding site residues. In conclusion, we propose analogues **3** and **2a** as highly promising NPP1 inhibitors.

INTRODUCTION

Two major families of ectonucleotidases, namely the ecto-nucleoside triphosphate diphosphohydrolases (NTPDases) family and the ecto-nucleotide pyrophosphatase/phosphodiesterase (NPPs) family terminate nucleotide signaling through the hydrolysis of nucleotide agonists of the P2X and P2Y receptors.[1, 2] The NTPDase family consists of eight Ca^{2+}/Mg^{2+}-dependent ectonucleotidases (NTPDase1-8) which hydrolyze extracellular nucleoside-5'-triphosphate and nucleoside-5'-diphosphate, to nucleoside 5'-monophosphate.[1] The NPP family consists of seven ecto-enzymes[3, 4] which exist as membrane glycoproteins with an extracellular divalent-ion containing active site,[5] yet, are also found extracellularly as secreted enzymes.[6] NPP1-3, the only nucleotide-hydrolyzing members of this group, have a wide tissue distribution,[6] and are capable of hydrolyzing phosphodiester and pyrophosphate bonds of nucleotides. NPPs are more specific for phosphodiester vs. phosphomonoester substrates. NPP1 and NPP3 both hydrolyze extracellular nucleoside di/triphosphates derivatives.[7] NPP1 can catalyze the hydrolysis of ATP to either ADP and Pi or AMP and PPi.[3] NPP2 has a much lower ATPase activity than NPP1/3.

NPP1-3 can control P2 and P1 receptor signaling because their enzymatic action results in the hydrolysis of signaling nucleotides and the generation of new messengers like AMP, adenosine or pyrophosphate.[6]

NPP1 is expressed in different tissues. It was reported to exist in bone (osteoblasts) and cartilage (chondrocytes) and has a role in regulating mineralization processes.[8] Extracellular pyrophosphate (ePPi), the product of ATP hydrolysis by NPP1, is a likely source of inorganic phosphate to sustain hydroxyapatite (HA) formation when

hydrolyzed by phosphatases, and is also a potent inhibitor preventing apatite mineral deposition and growth.[9] The main hydrolyzing agent of PP_i within chondrocytes is tissue non specific alkaline phosphatase (TNAP).[3] TNAP is a highly similar ectoenzyme to NPP1 containing a similar catalytic site and hydrolyzing its substrates in a similar mechanism.[5] Although TNAP's main substrate within chondrocytes is PP_i, TNAP can also act as a phosphodiesterase and hydrolyze nucleoside–5'-triphosphates (NTPs).[10] Although PPi is required to prevent ectopic mineralization, its overproduction leads to deposition of the pathological mineral calcium pyrophosphate dihydrate (CPPD), most often in the articular cartilage.[11, 12] This condition, known as chondrocalcinosis, frequently accompanies age-related osteoarthritis.[3]

A role for NPP1 in insulin receptor signaling has also been proposed.[13] Defective insulin-stimulated insulin receptor autophosphorylation in type 2 diabetes patients was found to result from an overexpression of NPP1.[13,14-16] In addition, NPP1 was found in human astrocytic brain tumors and was correlated with tumor gradation.[17-18]

The activity of NPP1 is endogenously regulated by AMP (*i.e.,* product inhibition).[8] Yet, non-endogenous NPP inhibitors have been scarcely reported. Recent reports suggested that quinazolin-4-piperidine-4-methyl sulfamide is a NPP1 inhibitor lacking binding affinity for hERG,[19] and that 1,3,4-oxadiazole (thiadiazole)-2 (3H)-thiones are non-competitive human NPP1 inhibitors with K_i values of 360 micromolar.[20] Previously, we reported that di-2'-deoxyadenosine-α,β-*δ*,ε-dimethylene-pentaphosphonate (Figure 1A), is an NPP1 inhibitor with an IC_{50} of 13 μM and a K_i of 9 μM.[21] In addition, we recently reported that adenosine 5'-α-borane-β,γ-methylene triphosphate (isomer A) (Figure 1B) is a selective inhibitor of NPP1 with a K_i of 0.5 μM.[22]

Here, we continue our search for highly potent and selective NPP1 inhibitors. Specifically, we describe the synthesis of a series of new ATP analogues bearing both phosphonate and thiophosphate modifications, the evaluation of their activities as NPP1 inhibitors, and their selectivity for NPP1 vs. other ectonucleotidases and representative adenine nucleotide binding receptors, $P2Y_{1,2,11}$ receptors. Furthermore, we performed docking simulations of the new analogues (Figure 2) to the catalytic site of a model of human NPP1 and analyzed the resulting poses to deduce the interaction pattern with binding site residues and the origin of NPP1 inhibitory activities.

RESULTS

Design and synthesis of potential NPP1 inhibitors

NPPs hydrolyze P_α-P_β phosphorodiester as well as P_β-P_γ phosphoroester bonds. In an attempt to confer hydrolytic stability and possibly inhibitory activity of nucleotide ligands at NPP1, we have designed compounds **1** and **2** in which the P_α phosphate moiety was modified to a thiophosphate group and a methylene or dichloromethylne group, respectively, was introduced between P_β and P_γ.

In compound **3** we replaced the nucleotide bridging P_α-P_β oxygen atom with a CH_2 group and modified the Pγ phosphate moiety to thiophosphate. The catalytic binding site of NPP1 was suggested to contain two Zn^{2+} ions,[23] although other reports suggested also activation by Mg^{2+} and Ca^{2+}-ions.[24, 25] Hence, thiophosphate groups were designed to chelate the tentative Zn^{2+} ions.[26] For this reason, we further replaced H8 of the adenine base in ATP by a thiol group, analogue **4**.

Synthesis of ATP-α-thio-β,γ-CX_2 analogues 1-2

Adenosine 5'-triphosphate-α-thio-β,γ-CX_2 analogues **1** and **2** were prepared from 2',3'-methoxymethylidene-adenosine, compound **5** (Scheme 1), to ensure a selective reaction of adenosine at 5'-OH. The 5'-OH of nucleoside **5** was activated with 2-chloro-4H-1,3,2-benzodioxaphosphorin-4-one to give compound **6** which was condensed with bis(tributylammonium) methylenediphosphonate or dichloromethylenediphosphonate to form the cyclic triphosphate intermediates, compound **7** (Scheme 1). Treatment of compound **7** with powdered sulfur yielded, after hydrolysis with triethylammonium bicarbonate (TEAB) buffer, analogues **1** or **2** in moderate yields (9-17%).

The identity and purity of the products were established by ^{1}H and ^{31}P NMR, ESI HR mass spectrometry, and HPLC in two solvent systems. The ^{31}P NMR spectra of analogues **1** and **2** showed a typical Pα signal as a doublet at about 43 ppm (J = 34 Hz). The ^{1}H NMR spectrum of analogue **1** showed methylene hydrogen atoms as a triplet at about 2.3 ppm (J = 20 Hz). Due to the chiral center at Pα, analogues **1** and **2** were each obtained as a pair of diastereoisomers in a 1:1 ratio. In both ^{1}H and ^{31}P NMR spectra, there was a slight difference between the chemical shifts of the diastereoisomers of analogues **1** and **2**. For instance, diastereoisomers **1a,b** (Figure 3), yielded two sets of signals for H8, at 8.67 and 8.62 ppm. These isomers were well separated by reverse-phase HPLC with about 6-10 min difference in their retention times. The first and second eluting isomers were designated as isomers A and B, respectively.

Assignment of the absolute configurations of 1a,b and 2a,b diastereoisomers

We employed ^{1}H NMR spectroscopy to elucidate the absolute configuration at Pα of **1a,b** and **2a,b** diastereoisomers. A difference in the chemical shift of H8 was observed between the two diastereoisomers of ATP-β,γ-methylene-α-S. The signal of H8 of isomer A in ^{1}H NMR spectrum was more shielded than that of the H8 of isomer B possibly due to the effect of the proximal negatively charged Pα group of thiophosphate (8.62 vs 8.67 ppm). Pα is much further away from H8 in isomer B than in isomer A (Figure 3). Thus, the *S*p configuration may be attributed to isomer A, analogue **1a**, and the *R*p configuration to isomer B, analogue **1b**.[27]

Synthesis of Pγ-thio-α,β-CH_2 ATP, analogue 3, and 8-SH-ATP, analogue 4

Adenosine 5'-triphosphate-α,β-CH_2-γ-thio, analogue **3,** was prepared in several steps from protected adenosine, compound **5**, (Scheme 2). 5'-OH of **5** was activated with tosyl chloride and a catalytic amount of dimethylamino pyridine. Adenosine 2',3'-methoxy methylidene-5'-tosyl, compound **8**, was phosphorylated with methylene diphosphonate bis(tributylammonium) salt to form 5'-adenosine diphosphonate compound **9**.[28] Next, the protecting group was removed with 10% HCl and then with 10% NH_4OH. Activation of compound **10** with carbonyl diimidazole (CDI) for 4-5 h resulted in phosphoroimidazolide intermediate, the yield of which was ca. 50% by NMR. Subsequently, MeOH was added to decompose the excess CDI, followed by addition of thiophosphate $(Bu_3NH)^+/(Oct_3NH)^+$ salt and $ZnCl_2$. The latter was added to protect the thiophosphate sulfur atom from reaction with phosphorimidazolide. Finally, compound **11** was obtained in 29% yield after LC separation.

The ^{31}P NMR spectrum of analogue **3** showed a typical Pγ signal as a doublet at about 39 ppm (J = 32 Hz). The ^{1}H NMR spectrum of analogue **3** showed methylene hydrogen atoms as a triplet at about 2.5 ppm (J = 20 Hz).

Analogue **4**, was obtained in two steps from 8-Br-adenosine (Scheme 3).[29] 8-Mercapto-adenosine, obtained in a quantitative yield from 8-Br-adenosine upon treatment with 10 equivalents of NaSH in wet DMF at 100 °C overnight, was 5'-triphosphorylated first by addition of $POCl_3$ in the presence of proton sponge in TMP for 3 h and then, by the addition of pyrophosphate in DMF for 2 h at -15°C, to give analogue nucleotide **4** at a 60% yield.

Analogues 1-3 are not substrates of NTPDase1, -2, -3, -8, NPP1, -3, or TNAP

Experiments were conducted with protein extracts from COS-7 cells transfected separately with an expression vector encoding each ectonucleotidase i.e., NPP1, NPP3 and NTPDase1, -2, -3, and -8. The protein extracts of non-transfected COS-7 cells exhibited less than 5% NTPDase or NPP activity compared with COS-7 cells transfected with NTPDases or NPPs, thus allowing the analysis of each ectonucleotidase in its native membrane bound form.[30]

Analogues **1-3** (100 μM, n=3) were stable to hydrolysis by NTPDase1, -2, -3 and -8 when compared to ATP (4.4-5.5% hydrolysis over 1 h, Table 1). Analogues **2** and **3** (100 μM) also were neither catabolized by NPP1 nor by NPP3. Analogue **1a** (100 μM) was fully stable to NPP1 hydrolysis and was hardly hydrolysed by NPP3 over 1h (~1%) compared to the physiological substrate ATP. Analogue **1b** was weakly hydrolyzed by both NPP1

and NPP3 (~4%). Analogue **4** was hydrolyzed by NPP1 and NPP3 at 32-54% over 1 h and therefore, was not studied further as an inhibitor of these enzymes.

In addition, the metabolic stability of the promising candidates, **2a** and **3,** was further proven by their resistance to enzymatic hydrolysis by TNAP. Compound **2a** was fully stable to TNAP hydrolysis during 1 h vs. 100% hydrolysis of ATP, and **3** was negligibly hydrolysed (2.5%) (data not shown).

Analogues 1-3 are selective inhibitors of NPP1

The effect of analogues **1-3** on NPP and NTPDase activities and their selectivity were tested using a synthetic substrate (pNP-TMP) as well as a natural substrate (ATP), respectively. Analogues **1-3** at (100 μM, n=3) effectively inhibited pNP-TMP (100 μM) hydrolysis by NPP1 by over 90% (Figure 4A). The hydrolysis of the physiological substrate ATP by NPP1 was inhibited more potently by analogues **2a** and **3** vs. **1a/b** and **2b** (Figure 4B). Similar inhibition was observed when osteocarcinoma cells (HTB85 cells, also known as SaOS 2) were used as a native source of NPP1 (Figure 4C). Analogues **1-3,** at 100 μM**,** were NPP1selective inhibitors, since they inhibited NPP3 activity by only 23-43% (Figure 4A, B).

Analogues **1a**, **1b**, **2a** and **2b** did not interfere with the hydrolysis of ATP by human NTPDase1, -2, -3 and -8 (Table 2). Analogue **3** at 100 μM inhibited human NTPDase1 and -3 by 60% and 40%, respectively (Table 2). Both compounds **2a** and **3** at 100 μM showed low inhibition of TNAP, 17% and 8% respectively.

We have estimated IC_{50} (a parameter that shows the ability of a molecule to inhibit an enzyme under specific conditions and substrate concentration), and inhibition constant K_i (a kinetic parameter that represents an absolute value for each tested inhibitor) towards NPP1. The kinetic parameters indicate that analogue **3** is the most potent inhibitor of NPP1 with K_i value of 20 nM (Table 3, Figure 5). Analogue **2a** was also a good NPP1 inhibitor exhibiting a K_i value of 685 nM. Under these experimental conditions the IC_{50}s of both analogues were also the lowest being 390 nM and 600 nM for **3** and **2a**, respectively (Table 3). Using the methods of Dixon (Figure 5A and Table 3) and Cornish-Bowden (Figure 5B and Table 3) that estimate dissociation constant for EIS complex (K_i'), we determined that the inhibitors **1b**-**3** presented in Table 3, showed mixed type inhibition, predominantly competitive.[31, 32]

Evaluation of analogues 1-3 as agonists of $P2Y_1$, $P2Y_2$, and $P2Y_{11}$ receptors

Adenine nucleotides are not only substrates of ectonucleotidases but are also potent agonists at $P2Y_1$, $P2Y_2$, and $P2Y_{11}$ G-protein-coupled receptors.[33] These receptors are expressed in many tissues and are involved in many diseases. Of relevance to the current study is the expression of P2Y receptors in bone tissues. $P2Y_1$ receptors are expressed in osteoclasts and osteoblasts,[30] $P2Y_2$ receptors are expressed in osteobloasts where they block bone formation[34] and the $P2Y_{11}$ receptors are expressed in human osteoclast cultures.[35] This expression pattern may lead to selectivity problems for inhibitors if they act as P2YR agonists.

With this in mind, we evaluated the activity of NPP1 inhibitors, analogues **1-3**, at $P2Y_{1,2,11}$ receptors. GFP (green fluorescent protein) constructs of human $P2Y_1$, $P2Y_2$ and

$P2Y_{11}$ receptors were expressed in 1321N1 astrocytoma cells, which lack endogenous expression of P2X and P2Y receptors.[36] These cells were then incubated with various concentrations of analogues **1**-**3**. The Ca^{2+} responses to analogues **1**-**3** were compared with ATP. Analogues **1**-**3** were weak agonists (EC_{50} > 10 μM) of the $P2Y_1$ receptor (Table 4). Analogues **1a** and **2a** were not agonists of the $P2Y_{11}$-receptor. In contrast, analogues **1b** and **3** were 7-fold more potent than the endogenous $P2Y_{11}$- receptor ligand, ATP (EC_{50} 6.7 μM) (Figure 6). In addition, analogue **2b** was a $P2Y_{11}$- receptor agonist (2-fold more active than ATP). Analogues **2a** and **3** (100 μM) had no activity, as agonists at $P2Y_2R$. These analogues did not inhibit the typical response to UTP observed for the $P2Y_2R$ in 1321N1 cells (data not shown).

Docking simulations at human NPP1

Docking simulations were used in order to provide insight into the inhibitory activities of the analogues studied in this work. We have previously reported a model of human NPP1 based on the recently solved structure of mouse NPP1[22] and demonstrated that docking simulations using Glide were able to successfully reproduce the crystallographic pose of AMP in this structure with a RMSD of 0.73 Å and to provide plausible binding mode for ATP in which it is stabilized within the binding site through an array of aromatic, hydrophobic, and H-bond interactions with binding site residues. These previous docking simulations suggest that Glide is a suitable docking tool for this system.

Analogues **1-3** were docked into the NPP1 site and their representative poses were analyzed. These were obtained by first clustering all poses obtained by the docking simulations within the binding site and then by selecting the pose which is closest to the

center of the largest cluster. The representative poses of all five analogues (**1-3**) were found to adopt ATP-like conformations, suggesting that they could compete with ATP for binding site interactions (Figure 7, Table S1). Furthermore, similar to ATP, all five analogues coordinate Zn1 through their P_α oxygen atom (although other chelation patterns were also observed). An excellent correlation (R^2 = 0.95; Figure 8a) was found between Boltzmann averaged Glide scores of the largest cluster and between experimental ΔΔG values (calculated from K_i values at the experimental temperature of 37°C using analogue **3** as a reference) for all five analogues considered in this work. Furthermore, this correlation was largely maintained when only the representative poses from each cluster were considered (R^2 = 0.8; Figure 8b). In addition, a very good correlation (R^2 = 0.95; Figure 8c) was found between the analogues' activities and the hydrogen bond term which forms part of Glide's scoring function. A detailed analysis of the interaction patterns of the representative poses of all analogues with binding site residues is provided in Table S1.

DISCUSSION

A series of ATP analogues modified at the $P_\alpha/P_\beta/P_\gamma$ positions by bridging methylene and thiophosphate moieties (analogues **1-3**) or by including a 8-SH group (analogue **4**) was designed and synthesized to identify potent and selective NPP1 inhibitors. Analogue **4** was hydrolyzed by NPP1 and NPP3 at about 50% the rate of ATP (Table 1), and therefore it could not serve as a good NPP inhibitor. Of the remaining compounds, ATP-α,β-CH_2-γ-S, **3**, was found to be an extremely potent NPP1 inhibitor (K_i 20 nM, Figure 5, Table 3) followed by ATP-α-S-β,γ-CCl_2, **2a** (K_i 685 nM, Figure 5, Table 3), while the

other three analogues were less active (**1b**, K_i 1.3 μM; **1a**, K_i 4.5 μM; **2b**, K_i 15 μM, Table 3).

In order to provide structural insight into these results as well as tools for the design of yet more potent NPP1 inhibitors, analogues **1**-**3** were docked into the binding site of our previously reported NPP1 model.[22] Similar to other non-hydrolysable ATP derivatives studied by us in the past,[22] the representative poses of all five analogues (**1a**, **b**, **2a**, **b** and **3**) adopt ATP-like conformations, suggesting that they could effectively compete with ATP for binding site interactions (Figure 7, Table S1). Furthermore, similar to ATP, all simulated analogues coordinate the Zn1 through their P_α oxygen atom (although other chelation patterns were also observed). While zinc is known to be a "thiophilic" ion, our docking results demonstrate preference for zinc chelation through the non-bridging oxygen atom of the phosphate chain rather than through the sulfur atom. Yet, we argue that this non-typical chelation pattern may be the consequence of binding site constraints. With this in mind we have searched the PDB for protein complexes where a ligand containing both oxygen and sulfur atoms chelates a zinc ion. Twenty four such complexes were found out of which seven demonstrated O-Zn chelation. Interestingly, out of this list of ligands, the two ligands most similar to analogues **1-3**, (ATP-γ-S, PDB code 3ZEU and a phosphorothioate derivative, PDB code 1KRP) show zinc chelation via oxygen. In the present study, the potential role of the binding site in controlling Zn^{2+}-chelation pattern is nicely demonstrated for the most active compound, analogue **3**. As the data in Table S1 clearly indicate, zinc chelation via the P_γ sulfur atom, rather than via P_α oxygen atom, results in loss of important interactions with binding site residues including hydrogen bonds with Thr256, Lys295, and Tyr340 and an important salt bridge

with Lys255. These findings suggest that the role of the sulfur atom may not be to enhance binding by providing better chelation to the zinc ion but rather by affecting the degree of ionization of the terminal phosphate. Indeed the pK_a of thiophosphate is 5.5 whereas that of phosphate is 6.5.[37]

The docking results were analyzed using a Boltzmann averaging of glide scores over the largest cluster of each analogue and resulted in an excellent correlation ($R^2 = 0.95$; Figure 8a) with experimental $\Delta\Delta G$ values calculated from the kinetic parameters (K_is). This correlation was largely maintained when considering only a single (representative) structure pose for each cluster ($R^2 = 0.8$; Figure 8b). The representative poses of all ligands considered in this work are given in Figure 7 and an analysis of their interaction patterns with binding site residues as well as key Glide scores (total score, H-bond score and electrostatic score) are given in Table S1. In particular, the hydrogen bond component of the scoring function shows an excellent correlation ($R^2 = 0.95$) with the experimental data (Figure 8c). This is reflected in the hydrogen bonding and salt bridge patterns of the representative poses of the different ligands (Figure 7 and Table S1). Thus, while the most active compound **3** is hydrogen bonded to five binding-site residues (Thr256x2, Asn277, Lys295, and Tyr340), and forms a salt bridge with Lys255, the less active analogues have fewer H-bonds (**2a**: two H-bonds with Asn277 and Tyr340; **1b**: two H-bonds with Asn277 and Lys295; **1a**: one H-bond with Asn277) while maintaining the salt bridge with Lys255, and the least active analogue has only two H-bonds and no salt bridge (**2b**: two H-bonds with Asn277 and Lys295). In addition, analogue **3** features the most favorable electrostatic energy component of the Glide score (-65.7 kcal/mol) although no clear correlation is observed between this score and the binding affinities

(Table 4 and S1). Presumably, for **1b** vs. **2b** the introduction of the bulkier chlorine atoms shifts the position of the **2b** analogue within the binding site leading to the loss of the important electrostatic interaction with Lys255.

Analogues **2a** (the second most active compound) and **2b** (the least active compound) differ only in the chirality at P_α (*S* and *R*, respectively). While this reversed chirality is reflected in the more favorable H-bond and salt bridge pattern of the more active compound (see above), it also leads to different exposures of polar surface areas to the solvent. As the data in Figure 9 indicate, analogue **2a** exposes a more polar "face" to the solvent than analogue **2b**. This in turn may lead to more favorable ligand-solvent interactions for this analogue and consequently to a stronger protein binding.

A detailed analysis of the representative poses of the five analogues does not provide a clear interpretation as to the role of the two chlorine atoms since they are not involved in specific interactions with binding site residues. These atoms were originally introduced into the ATP skeleton in order to reduce the pK_a of the terminal oxygen of the phosphonate moiety bringing it closer to that of phosphate (the pK_a of phosphonate, dichlorophosphonate and phosphate are 8.4, 6.7-7.0, and 6.5, respectively),[38, 39] making it a more potent inhibitor. This was indeed the case for analogues **1a** and **2a** (4.5 and 0.685 μM, respectively, Table 3) but not for analogues **1b** and **2b** (1.3 and 15.2 μM, respectively, Table 3).

Analogues **1-3** at 100 μM inhibited selectively NPP1 vs. NPP3 (Figure 4A), inhibiting the former by 90-100%, and the latter by only 23-43%, using pNP-TMP as the substrate. Analogues **2a** and **3** at 100 μM inhibited about 90% of ATP hydrolysis by NPP1 (Figure 4B). The results were confirmed by assays with osteocarcinoma cells (Figure 4C).

Analogues **2a** and **3** exhibited *Ki* and IC_{50} values of 685 nM and 600 nM, and 20 nM and 390 nM, respectively. IC_{50} values that do not parallel Ki_s values may perhaps result from difference in hydrophobic character of compounds **2a** and **3** under the experimental conditions that may influence the type of observed inhibition (see Fig. 7D, F and Table 3).

As previously reported,[22] the preferred binding of all analogues to NPP1 rather than to NPP3, could be readily explained by comparing the binding sites of the two proteins. In NPP1, a unique arrangement of Lys residues (seven in total) which is absent in NPP3 (a single binding site Lys residue), results in a highly positive electrostatic potential which renders this site more suitable for binding negatively charged nucleotides.

Analogues **1-2** at 100 μM had a minor inhibitory effect on NTPDase1, -2, -3, -8 activity (0-25% inhibition) (Table 2). In contrast, analogue **3** inhibited NTPDase1 by 60% and NTPDase3 by 40%. In addition, the two most promising candidates **2a** and **3** had a limited effect on TNAP activity showing minor inhibition (8-17%).

As adenine nucleotides are also the endogenous agonists of $P2Y_{1,2,11}$ receptors, we tested analogues **1-3** at these receptors involved in numerous physiological activities.[40, 41] Compounds **1a, b** did not activate the $P2Y_1$ receptor, consistent with earlier reports that a methylene modification tends to reduce agonist potency at P2Y receptors as compared to ATP.[42-44] Both ATP (pEC_{50} = 4.77) and ATP-γ-S (pEC_{50} 5.52) activate $P2Y_{11}$ receptor[45] with ATP-γ-S being the most potent agonist of the two.[30] Consistent with this, ATP-α,β-CH_2-γ-thio, **3**, was found here to be ~7-fold more potent than ATP at this receptor. This finding is also in agreement with our previously reported model of $hP2Y_{11}$-R and its preference for ATP-γ-S over ATP binding as a result of the tighter fit of the larger P_γ-S

moiety.[46] Adenosine 5'-triphosphate-α-thio-β,γ-CH_2 isomer B, **1b,** and adenosine 5'-triphosphate-α-thio-β,γ-CCl_2 isomer B, **2b,** showed ~7- and ~2-fold, respectively, higher potency than ATP at the $P2Y_{11}$ receptor. The respective isomers A, **1a** and **2a** were inactive at the $P2Y_{11}$ receptor.

This is in accordance with our previous findings[47] reporting that the $P2Y_{11}$ receptor prefers isomer B of Pα-substituted ATP derivatives over isomers A. Recently we found that adenosine 5'-triphosphate 2-propylthio-α-thio-β,γ-CCl_2, isomers A and B,[48] showed ~3- and ~4 fold, respectively, higher potency than ATP at the $P2Y_{11}$ receptor. In accordance with our findings presented here, the α-thio-β,γ-CCl_2-substituted ATP derivatives were very weak agonists at the $P2Y_1$ receptor, or not active at the $P2Y_2$ receptor. The nucleotides used in the present study lack the 2-propylthio modification of potent $P2Y_{11}$R agonists,[48] but have the α-thio β,γ-CCl_2 – substitution. Taken together, these results suggest that the α-thio β,γ-CCl_2 – substitution generally increases the affinity and selectivity of ATP derivatives at the $P2Y_{11}$ receptor.

Site-directed mutagenesis and computational analysis identified some amino acid residues responsible for the ligand recognition of the $P2Y_1$ and $P2Y_{11}$ receptor, as reported before. [27, 46, 49, 50] However, only little is known about the molecular structure of the binding pocket of all the P2Y receptors. Even though they belong to the same phylogenetic family, P2Y receptor subtypes show significant differences in amino acid sequences.[51, 52] $P2Y_1$, $P2Y_2$, and $P2Y_{11}$ receptors differ in their preference for the natural agonists.[53] Therefore, different EC_{50} values are expected for the nucleotide derivatives tested here (Table 4).

The newly identified NPP1 inhibitors were found to be highly potent, as compared to currently available inhibitors. Specifically, analogues **2a** and **3** were 525-fold and 18,000-fold, respectively, more potent human NPP1 inhibitors than the recently reported [4-(t-butyldimethylsilyloxy)-phenyl]-1,3,4-oxadiazole-2 (3H)-thione.[20] Likewise, analogue **3** was found to be 405-fold and 25-fold more potent than our previously reported NPP1 inhibitors - di-2'-deoxyadenosine-α,β-*δ*,ε-dimethylene-pentaphosphonate (Figure 1) [21] and adenosine-5'-O-(α-boranotriphosphate)-β,γ-CH_2 (K_i 0.5 μM; Figure 2),[44] respectively. The greater activity of analogue **3** relative to adenosine-5'-O-(α-boranotriphosphate)-β,γ-CH_2 could possibly be attributed to its ability to coordinate the M^{2+} (Zn1) ion through its P_α non-bridging oxygen atom. Based on docking results, such coordination is not possible for the borano compound since in this compound, the non-chelating borano group at P_α points towards the Zn1 ion.[22]

The kinetic data presented in this work coupled with the structural insight into the origin of the analogues' activities available from the docking simulations suggest that analogues **3** and **2a**, together with the NPP1 and NPP3 models, are good starting points for the design of efficacious and selective NPP1 inhibitors. Nevertheless, being ATP-based, these analogues are not classical "drug-like" compounds. Yet, related compounds such as thiazole-4-carboxamide adenine dinucleotide and Denufosol have found their way into clinical trials.[54, 55] Developing these compounds into drugs may require pro-drug approaches,[55] appropriate formulations and/or administration modes other than oral. However, even if these compounds will not be eventually developed into drugs they are still likely to serve as important mechanistic tools for the study of the complex process of mineralization.

Experimental

General. All commercial reagents were used without further purification, unless otherwise noted. All air- and moisture sensitive reactions were conducted in flame-dried, nitrogen-flushed, two-neck flasks sealed with rubber septa, and the reagents were introduced with a syringe. Progress of reactions was monitored by TLC using precoated Merck silica gel plates (60F-253). Reactants and products were visualized using UV light. Compounds were characterized by NMR using a Bruker AC-200, DPX-300, or DMX-600 spectrometer. ^{1}H NMR spectra were recorded at 200, 300, or 600 MHz. Nucleotides were characterized also by ^{31}P NMR in D_2O using 85% H_3PO_4 as an external reference on Bruker AC-200 and DMX-600 spectrometers. High-resolution mass spectra were recorded on an AutoSpec-E FISION VG mass spectrometer. Nucleotides were analyzed using electron spray ionization (ESI) on a Q-TOF microinstrument (Waters). Primary purification of the nucleotides was achieved on a LC (Isco UA-6) system using a column of Sephadex DEAE-A25, swollen in 1 M $NaHCO_3$ at 8°C for 24 h. The resin was washed with deionized water before use. LC separation was monitored by UV detection at 280 nm. Final purification of the nucleotides was achieved on a HPLC (Merck-Hitachi) system using a semipreparative reverse phase column [Gemini 5u C-18 110A, 250 mm X 10 mm, 5 μm (Phenomenex, Torrance, CA)]. The purity of the nucleotides was evaluated on an analytical reverse-phase HPLC column system [Gemini 5u C-18 110A, 150 mm X 3.60 mm, 5 μm (Phenomenex)] in two-solvent systems with either solvent system I or II.

Solvent system I consisted of (A) 100 mM triethylammonium acetate (TEAA) (pH 7) and (B) CH_3CN. Solvent system II consisted of (A) 46 mM PBS (pH 7.4) and (B) CH_3CN. The details of the solvent system gradients used for the separation of each product are provided below. The products, obtained as triethylammonium salts, were generally ≥95% pure. All reactants for moisture-sensitive reactions were dried overnight in a vacuum oven. 2',3'-O-Methoxymethylidene adenosine, compound **5**,[56] 5'-tosyl- adenosine, compund **8**,[56] α,β-methylene-ADP, compound **9**,[56] and 8-SH-ATP, compound **4**,[56] were prepared as previously described.

Adenosine 5'-Pα-thio-β,γ-(methylene)-triphosphate (analogues 1a,b). A solution of 2-chloro-4H-1,3,2-benzodioxaphosphorin-4-one (98 mg, 0.48 mmol) in anhydrous DMF (0.75 mL), was added via syringe to a solution of 2',3'-orthoformate protected adenosine (compound **5**) (100 mg, 0.32 mmol) and anhydrous pyridine (250 μL) in 0.5 mL of anhydrous DMF at 0 °C under nitrogen. After stirring at RT for 1 h, tributylamine (500 μL) was added, followed by a solution of bis-(tetrabutylammonium) methylenediphosphonate (68 mg, 0.38 mmol) in anhydrous DMF (0.5 mL). The reaction mixture was stirred at RT for 2 h then sulfur (21 mg, 0.64 mmol) was added at 0 °C. The solution color changed to orange and afterwards to brown. After stirring at room temperature for 1.5 h, the mixture was dripped to a cold 1 M TEAB solution (10 mL) until pH~7 was attained. The resulting mixture was stirred at room temperature for 30 min. During that time the color of the solution changed to yellow. The solution was extracted (2 X 10 mL) with ether. The aqueous phase was freeze-dried twice. The product was then deprotected by addition of 10% HCl until pH 2.3 was obtained and the mixture

was stirred for 3 h. Afterwards 24% NH_4OH was added to give pH~9 and the mixture was stirred for another 45 min and freeze-dried overnight.

The crude residue was separated on a DEAE-Sephadex A25 column with a linear gradient of ammonium bicarbonate (from 0.1 M to 0.4 M ammonium bicarbonate. Total gradient volume - 600 mL). The relevant fraction was freeze-dried for four times to afford 20 mg (9% yield) of adenosine 5'-Pα-thio-β,γ-(methylene)triphosphate ammonium salt. Final seperation of analogues **1a, b** (two diastereoisomers) was carried out by HPLC on a semipreparative reverse-phase column with a TEAA/CH_3CN gradient from 96.6:3.4 to 95:5 over 22 min at a flow rate of 4.5 mL/min: retention time (t_R) (isomer **1a**) = 15.8 min, t_R (isomer **1b**) = 21.4 min. Isomer **1a**: ^{1}H NMR (D_2O, 200 MHz) δ 8.62 (s, H-8, 1H), 8.27 (s, H-2, 1H), 6.15 (d, J = 6.0 Hz, H-1', 1H), 5.00 (m, H2', 1H), 4.60 (m, H-3', 1H), 4.42 (m, H-4', 1H), 4.28 (m, H-5' , 2H), 2.28 (t, J = 20.0 Hz, CH_2, 2H) ppm; ^{31} P NMR (D_2O, 81 MHz) δ 42.9 (d, J = 33.5 Hz, Pα-S, 1P), 13.0 (br m, Pγ and Pβ, 2P) ppm; TLC (2:7:11 NH_4OH/H_2O/2-propanol) R_f = 0.22. The following purity data were obtained on an analytical column: t_R = 6.48 min (96% purity) using solvent system I with a TEAA/CH_3CN isocratic elution 95:5 over 10 min at a flow rate of 1 mL/min; t_R = 2.94 min (95% purity) using solvent system II with a PBS/CH_3CN isocratic elution 98:2 over 8 min at a flow rate of 1 mL/min. Isomer **1b**: ^{1}H NMR (D_2O, 200 MHz) δ 8.67 (s, H-8, 1H), 8.25 (s, H-2, 1H), 6.15 (d, J = 6.0 Hz, H-1', 1H), 5.00 (m, H2', 1H), 4.59 (m, H-3', 1H), 4.41 (m, H-4', 1H), 4.28 (m, H-5' , 2H), 2.31 (t, J = 21.0 Hz, CH_2, 2H) ppm; ^{31} P NMR (D_2O, 81 MHz) δ 43.2 (d, J = 32.4 Hz, Pα-S, 1P), 13.2 (br s, Pγ, 1P), 11.9 (br d, Pβ, J = 32.4 Hz, 1P) ppm; HRMS ESI (negative) *m/z*: calculated for $C_{11}H_{17}N_5O_{11}P_3S^-$ 519.9864, found 519.9853, low resolution mass was measured for both isomers

andHRMS was measured for one of the isomers; TLC (2:7:11 NH_4OH/H_2O/2-propanol) $R_f = 0.22$. The following purity data were obtained on an analytical column: $t_R = 9.12$ min (97% purity) using solvent system I with a TEAA/CH_3CN isocratic elution 95:5 over 15 min at a flow rate of 1 mL/min; $t_R = 4.17$ min (97% purity) using solvent system II with a PBS/CH_3CN isocratic elution 98:2 over 10 min at a flow rate of 1 mL/min.

Adenosine 5'-Pα-thio-β,γ-(dichloromethylene)triphosphate (analogues 2a, b)

A solution of 2-chloro-4H-1,3,2-benzodioxaphosphorin-4-one (117 mg, 0.58 mmol) in anhydrous DMF (1 mL), was added via syringe to a solution of 2',3'-orthoformate protected adenosine (compound **5**) (100 mg, 0.32 mmol) and anhydrous pyridine (260 μL) in 1.5 mL of anhydrous DMF at 0 °C under nitrogen. After stirring at RT for 1 h, tributylamine (626 μL) was added, followed by a solution of bis-(tetrabutylammonium) dichloromethylendiphosphonate (127 mg, 0.42 mmol) in anhydrous DMF (1 mL). The reaction mixture was stirred at RT for 2 h then sulfur (25 mg, 0.77 mmol) was added at 0 °C. The solution color changed to orange and then to brown while stirring at RT for 1.5 h. The mixture was dripped to a cold 1 M TEAB solution (10 mL) until pH~7 was attained. The resulting mixture was stirred at RT for 30 min. During that time the color of the solution changed to yellow. The solution was extracted with ether (2 X 10 mL). The aqueous phase was freeze-dried twice. The product was then deprotected by addition of 10% HCl until pH 2.3 was obtained and the mixture was stirred for 3 h. Afterwards 24% NH_4OH was added to give pH~9 and the mixture was stirred for another 45 min and freeze-dried overnight.

The crude residue was separated on a DEAE-Sephadex A25 column with a linear gradient of ammonium bicarbonate (from 0.1 M to 0.4 M ammonium bicarbonate. Total

gradient volume - 600 mL). The relevant fraction was freeze-dried for four times to afford 43 mg (17% yield) of adenosine 5'-Pα-thio-β,γ-(dichloromethylene)triphosphate ammonium salt. Final separation of analogues **2a,b** (two diastereoisomers) was carried out by HPLC on a semipreparative reverse-phase column with a TEAA/CH_3CN gradient from 96.5:3.5 to 95.5:4.5 over 31 min at a flow rate of 4.5 mL/min: t_R (isomer **2a**) = 20.3 min, t_R (isomer **2b**) = 30.6 min. Isomer **2a**: ^{1}H NMR (D_2O, 200 MHz) δ 8.72 (s, H-8, 1H), 8.29 (s, H-2, 1H), 6.16 (d, J= 6.0 Hz, H-1', 1H), (H2' and H-3' signals are hidden by the water signal at 4.78), 4.63 (m, H-4', 1H), 4.35 (m, H-5' , 2H), 3.35 (t, Et_3N , 24H), 2.05 (s, AcOH , H), 1.42 (d, Et_3N , 36H) c; ^{31}P NMR (D_2O, 81 MHz) δ 44.0 (d, J = 35.4 Hz, Pα-S, 1P), 8.0 (d, J = 19.3 Hz, Pγ, 1P), -1.0 (dd, J = 19.3 Hz, J = 35.4 Hz, Pβ, 1P) ppm; HRMS ESI (negative) *m/z*: $C_{11}H_{15}Cl_2N_5O_{11}P_3S^-$ calculated 587.9084, found 587.9073, low resolution mass was measured for both isomers and HRMS was measured for one of the isomers; TLC (2:7:11 NH_4OH/H_2O/2-propanol) Rf = 0.35. The following purity data were obtained on an analytical column: t_R = 9.5 min (99% purity) using solvent system I with a TEAA/CH_3CN isocratic elution 96:4 over 15 min at a flow rate of 1 mL/min; t_R = 3.35 min (99% purity) using solvent system II with a PBS/CH_3CN isocratic elution 98:2 over 8 min at a flow rate of 1 mL/min. Isomer **2b**: ^{1}H NMR (D_2O, 200 MHz) δ 8.65 (s, H-8, 1H), 8.29 (s, H-2, 1H), 6.16 (d, J= 6.2 Hz, H-1', 1H), (H2' signal is hidden by the water signal at 4.78), 4.64 (m, H-3', 1H), 4.45 (m, H-4', 1H), 4.38 (m, H-5' , 2H), 3.15 (t, Et_3N, 24H), 2.05 (s, CH_3CO_2H, 3H), 1.38 (d, Et_3N, 36H) ppm; ^{31} P NMR (D_2O, 81 MHz) δ 43.9 (d, J = 35.5 Hz, Pα-S, 1P), 8.00 (d, J = 19.1 Hz, Pγ, 1P), -0.9 (dd, J = 19.1 Hz, J = 35.5 Hz, Pβ, 1P) ppm; TLC (2:7:11 NH_4OH/H_2O/2-propanol) R_f = 0.36. The following purity data were obtained on an analytical column: t_R = 10.0 min

(98% purity) using solvent system I with a TEAA/CH_3CN isocratic elution 95:5 over 15 min at a flow rate of 1 mL/min; t_R = 4.54 min (98% purity) using solvent system II with a PBS/CH_3CN isocratic elution 98:2 over 10 min at a flow rate of 1 mL/min.

Adenosine 5' -α,β-methylene-γ-thio-triphosphate (analogue 3). α,β-Methylene-ADP$(Bu_3NH)^+$/$(Oct_3NH)^+$ and thiophosphate$(Bu_3NH)^+$/$(Oct_3NH)^+$ salts were prepared by applying the corresponding phosphate deriviatives through a column of activated Dowex 50WX-8 (200 mesh, H^+ form). The eluate was collected in an ice-cooled flask containing tributylamine, tri-n-octylammine (1 eq) and EtOH. The resulting solution was freeze-dried to yield α,β-methylene-ADP$(Bu_3NH)^+$/$(Oct_3NH)^+$ and thiophosphate$(Bu_3NH)^+$/$(Oct_3NH)^+$ salts, each as a viscous oil.

Adenosine-5'- α,β-methylene diphosphate tributylammonium and tri-n-octylammonium salt (75 mg, 0.17 mmol) were suspended in anhydrous DMF (2 mL), 1,1'-carbonyldiimidazole (260 mg, 1.64 mmol) was added at RT and the mixture was stirred for 5 h. Next, dry MeOH (66 μL) was added and the reaction was stirred for 8 min, followed by addition of anhydrous $ZnCl_2$ (220 mg, 1.60 mmol) and thiophosphate tributylammonium and tri-n-octylammonium salt (170 mg, 0.98 mmol) in dry DMF (1 mL) were added. After 3 h, the reaction was added to EDTA solution (580 mg, 1.5 mmol in 20 mL of water), brought to pH~7 with triethylammonium bicarbonate and the solution was freeze-dried overnight. The residue was separated on a DEAE-Sephadex A25 column with an isocratic elution of ammonium bicarbonate (from 0 to 0.4 M ammonium bicarbonate. Total gradient volume - 600 mL.). The solution was freeze-dried for four times to afford adenosine-5'-triphosphate-α,β-methylene-γ-thiophosphate ammonium salt (30 mg, 29% yield). Final purification of analogue **3** was carried out by HPLC on a

semipreparative reverse-phase column, using isocratic elution of 4% CH_3CN, 96% TEAA over 15 min at a flow rate of 4.5 mL/min: t_R = 10.25 min; ^{1}H NMR (D_2O, 200 MHz) δ: 8.58 (s, H-8, 1H), 8.26 (s, H-2, 1H), 6.09 (d, J= 5.8 Hz, H-1', 1H), 4.90 (m, H2', 1H), 4.56 (m, H-3', 1H), 4.36 (m, H-4', 1H), 4.20 (m, H-5' , 2H), 3.20 (t, Et_3N , 24H), 2.48 (t, J=20.00 Hz, CH_2, 2H), 1.30 (d, Et_3N, 36H) ppm; ^{31} P NMR (D_2O, 81 MHz) δ: 39.0 (d, J = 32 Hz, Pγ-S, 1P), 18.2 (d, J = 9 Hz, Pα, 1P), 6.9 (dd, J = 9 Hz, J = 32 Hz, Pβ, 1P) ppm; HRMS ESI (negative) *m/z*: $C_{11}H_{17}N_5O_{11}P_3S^{2-}$ calculated 519.9853, found 519.9820; TLC (2:7:11 NH_4OH/H_2O/2-propanol) R_f = 0.30. The following purity data were obtained on an analytical column: t_R = 5.23 min (90% purity) using solvent system I with a TEAA/CH_3CN isocratic elution 96:4 over 10 min at a flow rate of 1 mL/min; t_R = 6.72 min (93% purity) using solvent system II with a PBS/CH_3CN isocratic elution 97:3 over 10 min at a flow rate of 1 mL/min.

Plasmids

The plasmids used in this study have all been described in published reports: human NTPDase1 (GenBank accession no. U87967)[57], human NTPDase2 (NM_203368)[58], human NTPDase3 (AF033830)[59], human NTPDase8 (AY330313)[60], human NPP1 (NM_006208)[61] and human NPP3 (NM_005021)[62].

Cell culture and transfection

Ectonucleotidases were expressed by transiently transfecting COS-7 cells in 10 cm plates by use of Lipofectamine (Invitrogen, Burlington, ON, Canada), as previously described.[63] Briefly, 80–90% confluent cells were incubated for 5 h at 37°C in Dulbecco's modified Eagle's medium nutriment mix F-12 (DMEM/F-12) in the absence of fetal bovine serum (FBS) with 6 μg of plasmid DNA and 23 μL Lipofectamine reagent. The reaction was

stopped by the addition of an equal volume of DMEM/F-12 containing 20% FBS and the cells were harvested 33–72 h later.

Preparation of membrane fraction

For the preparation of protein extracts, transfected cells were washed three times with Tris-saline buffer at 3°C, collected by scraping in the harvesting buffer (in mM, 95 NaCl, 0.1 phenylmethylsulphonyl fluoride (PMSF) and 35 Tris at pH 7.5), and washed twice by 300 × g centrifugation for 10 min at 3°C. Cells were resuspended in the harvesting buffer containing 10 $mg \cdot mL^{-1}$ aprotinin and sonicated. Nuclei and cellular debris were discarded by centrifugation at 300 × g for 10 min at 3°C and the supernatant (crude protein extract) was aliquoted and stored at –80°C until used for activity assays. Protein concentration was estimated by the Bradford microplate assay using bovine serum albumin (BSA) as a standard of reference.[64]

NPPs and TNAP stability assay

Evaluation of the hydrolysis percentage (compared to ATP) of analogues **1**-**4** by human NPP1,3 and of **2a** and **3** by TNAP was conducted at 37°C in incubation buffer 0.573 mL containing: 1 mM $CaCl_2$, 130 mM NaCl, 5 mM KCl, and 50 mM Tris (pH 8.5 for NPPs and pH 9 for TNAP) with or without lysates of cells expressing NPP1,3 or TNAP. Analogues **1**-**4** were used at a final concentration of 100 μM. Recombinant human NPP1,3 or TNAP cell lysates were added to the above mixture and preincubated at 37°C for 3 min. The reaction was initiated by addition of the analogues or ATP (control). The reaction was stopped after 1 h by addition of 0.375 mL ice-cold 1 M perchloric acid. The samples were centrifuged for 1 min at 13 000 g. Supernatants were neutralized with 2 M KOH (0.136 mL) at 4°C and centrifuged for 1 min at 13000 g. Each mixture sample was

filtered and freeze-dried once for storage overnight. The samples were dissolved in HPLC water (0.2 mL) and filtered again. An aliquot of 20 μL was separated by reverse-phase HPLC to evaluate the nucleotide content of each reaction sample.

Separation and quantification of nucleotides by HPLC

An aliquot of 20 μL of the reaction products (described above) was used for nucleotide analysis on an analytical reverse-phase HPLC column [Gemini 5u C-18 110A, 150 mm X 3.60 mm, 5 μm (Phenomenex)]. Analogues **1-4** and their hydrolysis products were separated with a mobile phase consisting of 100 mM TEAA (99-90%, pH 7.0), and 1-10% CH_3CN, at a flow rate of 1 mL/min for 20 min. Separated nucleotides were detected by UV absorption at 260 nm, identified, and quantified by their peak integration and by comparison of the retention times with those of appropriate standards.

Inhibition of NTPDase (EC 3.6.1.5) - activity assays

Activity was measured as described previously[1] in 0.2 mL of Tris-Ringer buffer (in mM), 120 NaCl, 5 KCl, 2.5 $CaCl_2$, 1.2 $MgSO_4$, 25 $NaHCO_3$, 5 glucose, 80 Tris, pH 7.3) at 37°C with or without analogues **1-3** (final concentration 100 μM), and with or without 100 μM ATP as a substrate. The analogues were added alone when tested as potential substrate, and with ATP when tested for their effect on nucleotide hydrolysis. NTPDases protein extracts were added to the incubation mixture and pre-incubated at 37°C for 3 min. The reaction was initiated by the addition of substrate (ATP and/or analogues **1-3**) and stopped after 15 min with 50 μL of malachite green reagent. The released inorganic phosphate (Pi) was measured at 630 nm according to Baykov et al.[65]

Inhibition of NPP and TNAP (EC 3.1.4.1; EC 3.6.1.9) - activity assays

Evaluation of the effect of analogues **1-3** on human NPP1, and -3 activity was carried out either with pNP-TMP or ATP as the substrate.[61] pNP-TMP hydrolysis was carried out at 37°C in 0.2 mL of the following incubation mixture: in mM, 1 $CaCl_2$, 130 NaCl, 5 KCl and 50 Tris, pH 8.5, with or without analogues **1-3** and/or substrates. Substrates and analogues **1-3** were all used at the final concentration of 100 μM. Recombinant human NPP1 or NPP3 cell lysates were added to the incubation mixture and pre-incubated at 37°C for 3 min. The reaction was initiated by the addition of the substrate. For pNP-TMP hydrolysis, the production of p-nitro-phenol was measured at 310 nm, 15 min after the initiation of the reaction. The type of inhibition, IC_{50}, K_i and K_i' were calculated by plotting the data of three independent experiments using pNP-TMP as substrate according to Dixon and Cornish-Bowden methods.[31, 32]

Evaluation of the activities of human NPP1, NPP3, and TNAP with ATP and analogues **1-3** was carried out at 37°C in 0.2 mL of the following mixture: (in mM) 1 $CaCl_2$, 140 NaCl, 5 KCl, and 50 Tris, pH 8.5 for NPPs and pH 9 for TNAP. Human NPP1, NPP3 or TNAP extract was added to the reaction mixture and pre-incubated at 37°C for 3 min. The reaction was initiated by addition of ATP or analogues **1-3** at a final concentration of 100 μM. The reaction was stopped after 20 min by transferring a 0.1 mL aliquot of the reaction mixture to 0.125 mL ice-cold 1 M perchloric acid. The samples were centrifuged for 5 min at 13,000 g. Supernatants were neutralized with 1 M KOH at 4°C and centrifuged for 5 min at 13,000 g. An aliquot of 20 mL was separated by reverse-phase HPLC to evaluate the degradation of ATP and analogues **1-3** using the conditions described above.

Activity assays at the surface of intact HTB-85 cells were carried out in 0.5 mL of the incubation mixture in 24-well plates. Reaction was initiated by the addition of pNP-TMP to obtain a final concentration of 100 μM. After 20 min, 0.2 mL of the reaction mixture was transferred to a 96 well plate and the production of para-nitrophenol was measured at 410 nm as described above.

Calcium Measurements

Human 1321N1 astrocytoma cells transfected with the respective plasmid for GFP-P2Y-R expression were plated on glass bottom dishes and grown to approximately 80% density, an incubated with 2 μM fura 2/AM and 0.02% pluronic acid in HBSS (Hanks balanced salt solution: 5.44 mM KCl, 0.44 mM KH_2PO_4, 0.34 mM NaH_2PO_4, 0.49 mM $MgCl_2$, 0.41 mM $MgSO_4$, 132 mM NaCl, 5.56 mM glucose, Hepes 10 mM/Tris pH 7.4) for 30 min at 37°C. The cells were superfused (1 mL/min, 37°C) with different concentrations of nucleotide in HBSS. The nucleotide-induced change of $[Ca^{2+}]_i$ was monitored by detecting the respective emission intensity of fura 2/AM at 510 nm with 340 nm and 380 nm excitations.[66] The average maximal amplitude of the responses and the respective standard errors were calculated from the ratio of the fura 2/AM fluorescence intensities with excitations at 340 nm and 380 nm. Microsoft Excel (Microsoft Corp., Redmond, WA, USA) and SigmaPlot (SPSS Inc., Chicago, IL, USA) were used to derive the concentration-response curves and EC_{50} values from the average response amplitudes obtained in at least three independent experiments.[47, 49] Only cells with a clear GFP-signal that yielded typical calcium response kinetics upon agonist pulse application were included in the data analysis. The GFP-tagged P2Y receptors are suitable for pharmacological and physiological studies, as previously reported.[46, 67, 68]

Molecular modeling

A 3-dimensional (3D) model of human NPP1 was previously reported.[22] This model was used for the docking of analogues **1-3**. Prior to docking, the protein structure was prepared using the protein preparation wizard in Discovery Studio version 3.5.[69] Docking simulations were performed using Glide[70, 71] as implemented in Maestro 9.0.[72] Glide's grid box was centered on the binding site as deduced from the mouse NPP1 crystal structure. A docking grid was generated within the docking box and ligands were docked into the binding site using Glide's Extra Precision (XP) option with default parameters values.[73] Following docking, the resulting poses were clustered in Maestro using all heavy atoms along the analogues' "backbone" and the poses closest to the center of the largest clusters were taken as representatives. Boltzmann averaged energies were calculated over poses comprising the largest cluster at T = 37°C.

Supporting Information Available: Table of interactions between analogues **1a, b, 2 a, b**, and **3** in their representative poses with binding site residues within the catalytic site of the human NPP1 model. This material is available free of charge via the internet at http://pubs.acs.org

Figures, Schemes, and Tables

Figure 1. Dinucleotide and nucleotide analogues previously studied as potential NPP1 inhibitors. A. Di-2'-deoxyadenosine-α,β-*δ*,ε-dimethylene-pentaphosphonate B. ATP-5'-O-(α-borano)-β,γ-CH_2.

Figure 2. Adenosine 5'-triphosphate analogues studied here as potential NPP1 inhibitors.

Figure 3. *S*p and *R*p configurations are attributed to ATP-5'-α-S-β,γ-CH_2 diastereoisomers **1a** and **1b**, respectively.

Figure 4. Analogues **1-3** (100 μM) inhibit NPP activities. Activity of human NPP1 (hNPP1) and NPP3 (hNPP3) was tested with pNP-TMP (A, C) or ATP (B) as the substrate at 100 μM. The 100% activity with pNP-TMP alone was 48 ± 4 and 32 ± 2 [nmol *p*-nitrophenol·min^{-1}·mg $protein^{-1}$] for NPP1 and NPP3, respectively (A). The 100% activity with ATP alone was 153 ± 6 and 110 ± 5 [nmol *nucleotide*·min^{-1}·mg $protein^{-1}$] for NPP1 and NPP3, respectively (B). Data presented are the mean ± SD of 3 experiments carried out in triplicates. C**)** Analogues **1-3** inhibit NPP activity at the surface of HTB85 cells. The 100% NPP activity was set with the substrate alone and was 1.3 ± 0.04 [nmol *p*-nitrophenol·min^{-1}·well]. Data presented are the means ±SD of results from 3 experiments carried out in triplicates.

Figure 5. $K_{i,app}$ determination using Dixon (A) and Cornish-Bowden (B) plot, of human NPP1 by analogue **2a** and **3**. pNP-TMP concentrations were 25, 50 and 100 μM, and the inhibitor concentrations were 0, 25, 50 and 100 μM. The data of one representative experiment out of 3 is shown.

Figure 6. Activity of analogues **1b**, **2b** and **3** at the $P2Y_{11}R$. Data were obtained by determining the ligand-induced change in $[Ca^{2+}]_i$ in 1321N1 cells stably expressing the

human GFP-P2Y$_{11}$R. Cells were pre-incubated with 2 μM fura-2 AM for 30 min and change in fluorescence (ΔF340 nm/F380 nm) was detected.

Figure 7. Homology model of human NPP1 and representative poses for analogues **1-3**. A) 3D model of human NPP1 with ATP docked into its catalytic site. The protein is shown as a ribbon diagram color coded according to its secondary structure. The two tentative Zn ions are shown as orange spheres and the ATP molecule is depicted in blue. B-F) Representative poses of analogues **1a**, **1b**, **2a**, **2b** and **3**, respectively, in the binding site of the human NPP1 model. The two Zn ions are shown as orange spheres and the ligands are colored according to atom types (nitrogen atoms are colored in blue; oxygen atoms are colored in red; carbon atoms are colored in grey; phosphate atoms are colored in purple). H-bonds and π-interactions are shown in green and orange, respectively.

Figure 8. Correlation between binding free energies (kcal/mol; derived from the experimentally determined K_i values at 37°C) and (A) Boltzmann averaged Glide scores (kcal/mol) over the largest clusters; (B) Glide scores (kcal/mol) for the representative poses of analogues **1-3**, and (C) The H-bond component of the Glide score kcal/mol) ΔΔG values were calculated using analogue **3** as a reference.

Figure 9. Electrostatic potential of analogues **2a** and **2b**. Electrostatic potentials of analogue **2a** (A) and **2b** (B) within the human NPP1 model were calculated on their respective molecular surfaces. The enhanced negative potential (red) of the solvent exposed surface area corresponding to analogue **2a** in comparison with analogue **2b** (circled in green) is clearly visible.

Scheme 1. Synthesis of ATP-α-S-β,γ-(methylene)triphosphate analogues (**1a,b**/**2a,b**)

Scheme 2. Synthesis of ATP-α,β-methylene-γ-thiophosphate (**3**)

Scheme 3. Synthesis of 8-SH-ATP (**4**)

Table 1. Hydrolysis of analogues **1-4** by human ectonucleotidases.

Table 2. Effect of analogues **1-3** on human NTPDase1, -2, -3, -8 activity.

Table 3. Kinetic parameters and IC_{50} of NPP1 inhibition.

Table 4. EC_{50} values for $[Ca^{2+}]_i$ elevation by analogues **1-3**, mediated by $P2Y_{1,11}$ – receptors.

Figure 1

A

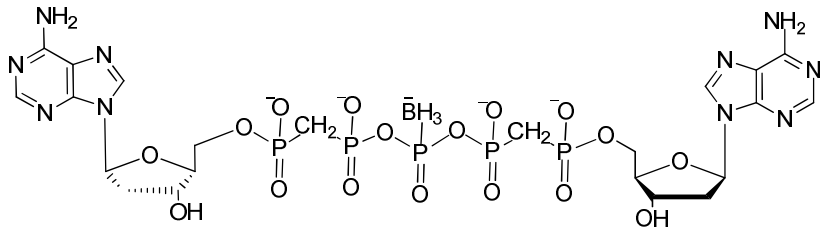

B.

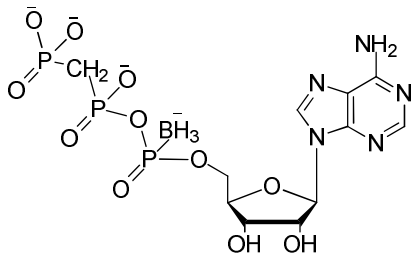

Figure 2

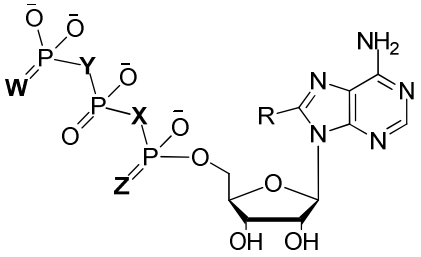

1 X = O Y = CH_2 Z = S R = H W = O
2 X = O Y = CCl_2 Z = S R = H W = O
3 X = CH_2 Y = O Z = O R = H W = S
4 X = O Y = O Z = O R = SH W = O

Figure 3

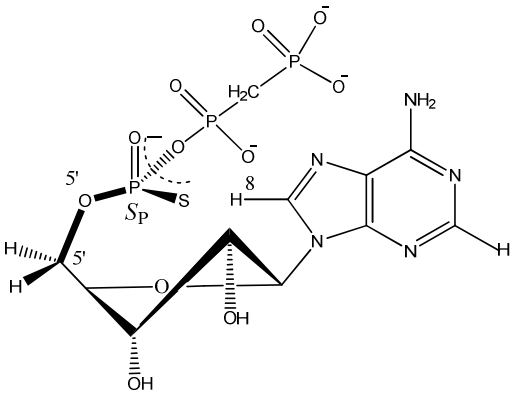

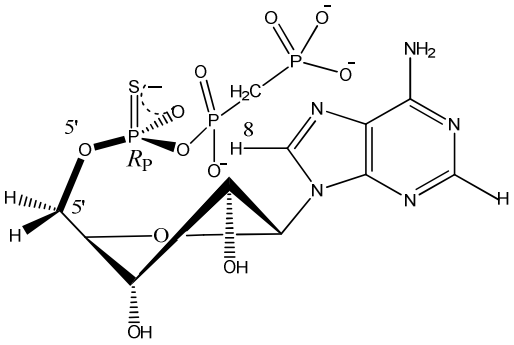

Figure 4

A. pNP-TMP

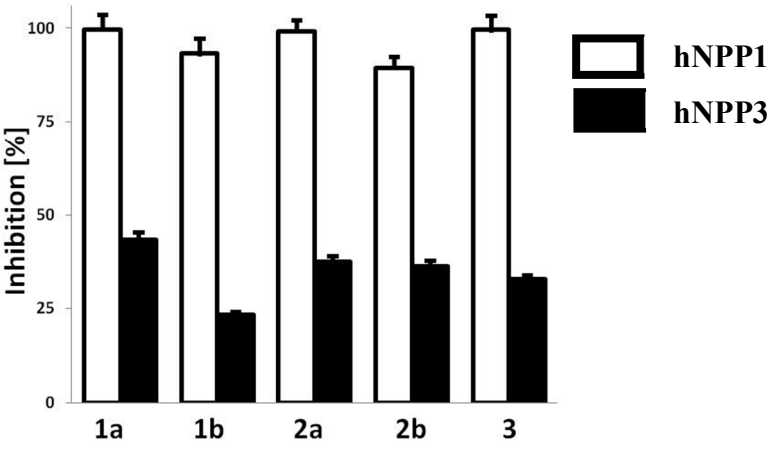

B. ATP

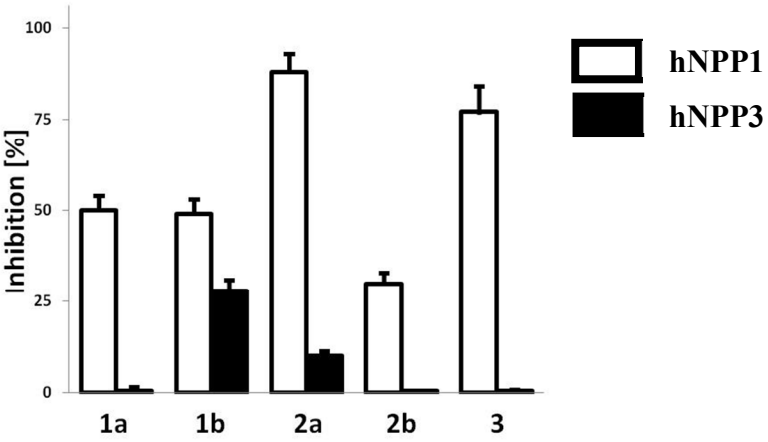

C. pNP-TMP with HTB85

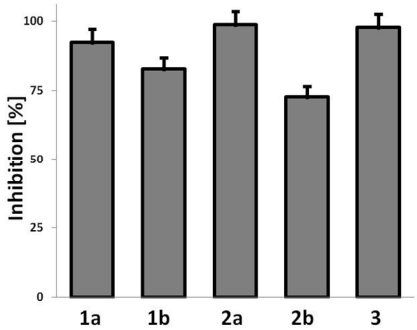

Figure 5

A.

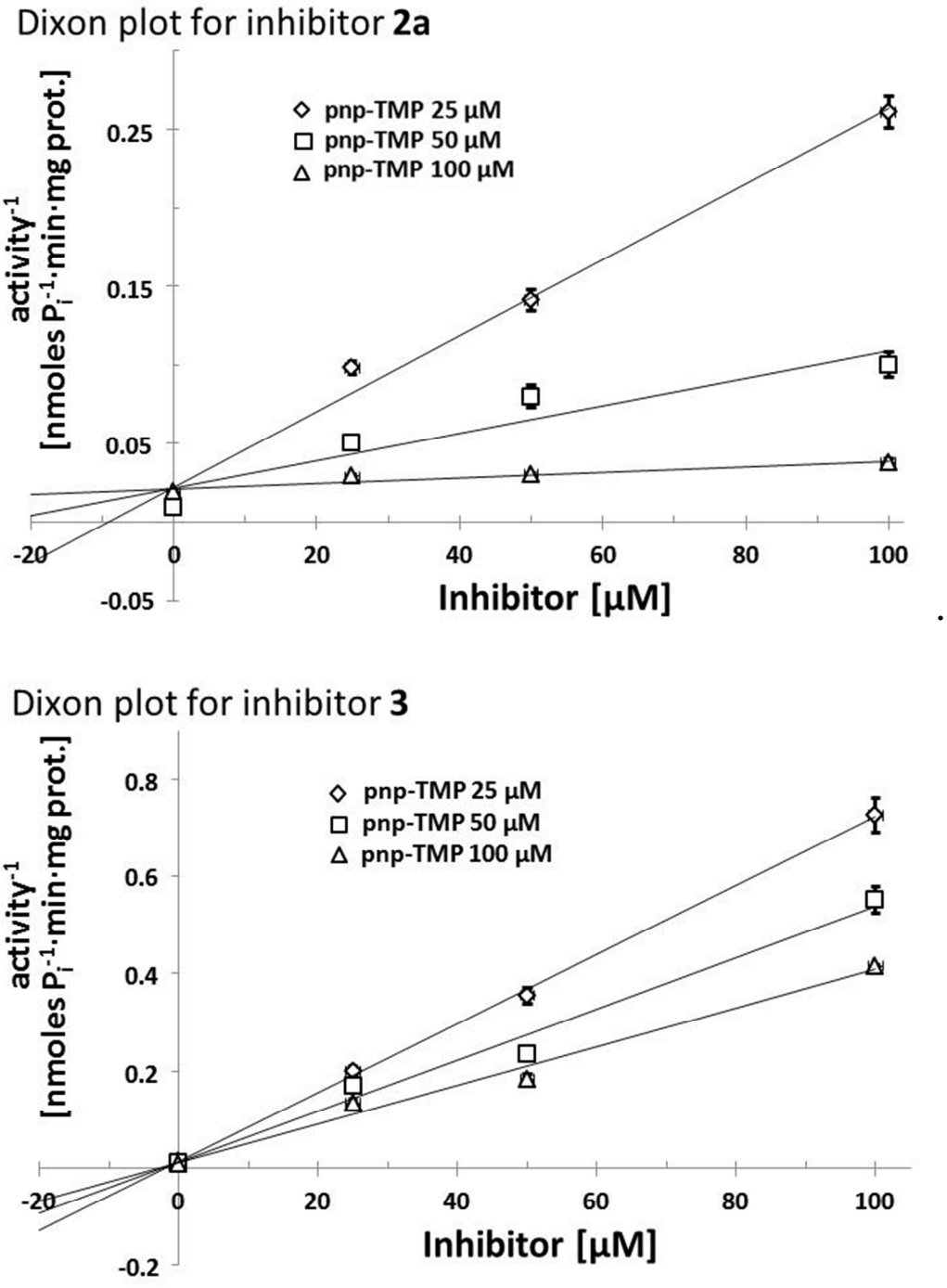
Dixon plot for inhibitor 2a
activity-1
[nmoles Pi-1·min·mg prot.]
pnp-TMP 25 µM
pnp-TMP 50 µM
pnp-TMP 100 µM
0.25
0.15
0.05
-0.05
-20
0
20
40
60
80
100
Inhibitor [µM]
Dixon plot for inhibitor 3
activity-1
[nmoles Pi-1·min·mg prot.]
pnp-TMP 25 µM
pnp-TMP 50 µM
pnp-TMP 100 µM
0.8
0.6
0.4
0.2
-0.2
-20
0
20
40
60
80
100
Inhibitor [µM]

B.

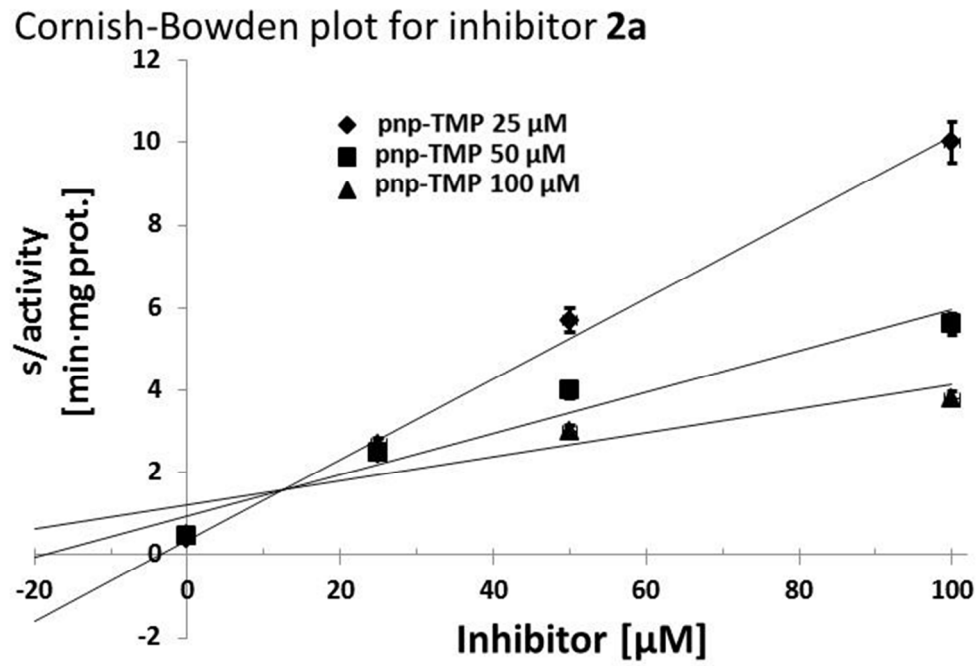
Cornish-Bowden plot for inhibitor 2a
pnp-TMP 25 µM
pnp-TMP 50 µM
pnp-TMP 100 µM
s/activity [min·mg prot.]
Inhibitor [µM]
12
10
8
6
4
2
0
-2
-20
0
20
40
60
80
100

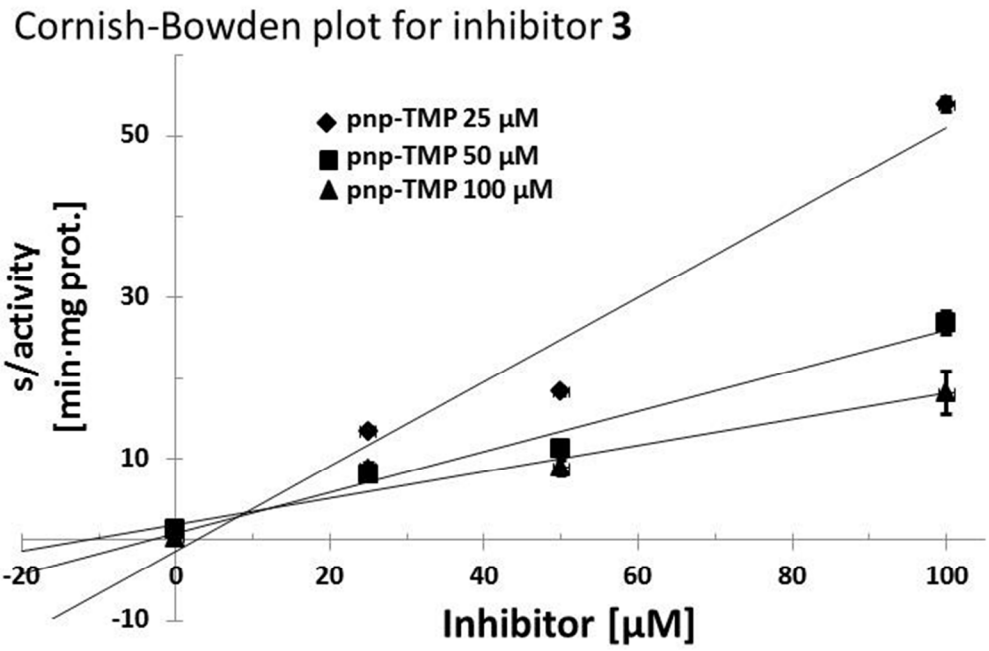
Cornish-Bowden plot for inhibitor 3
pnp-TMP 25 µM
pnp-TMP 50 µM
pnp-TMP 100 µM
s/activity [min·mg prot.]
Inhibitor [µM]
50
30
10
-10
-20
0
20
40
60
80
100

Figure 6.

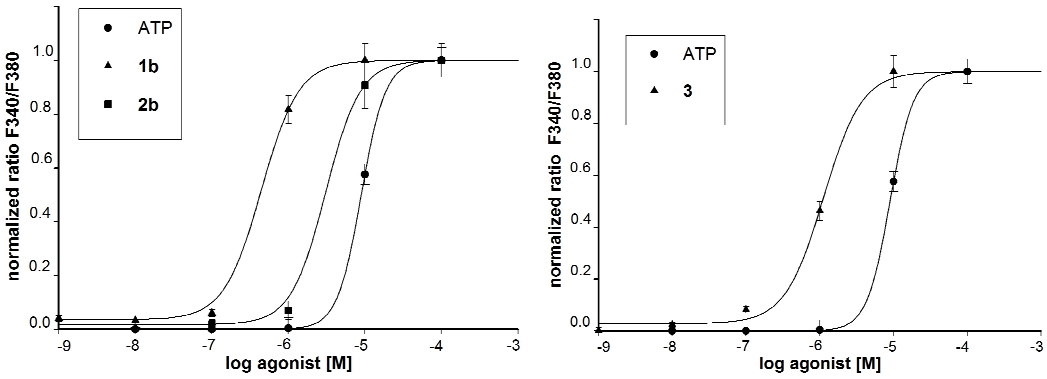
ATP
1b
2b
normalized ratio F340/F380
log agonist [M]
ATP
3
normalized ratio F340/F380
log agonist [M]

Figure 7

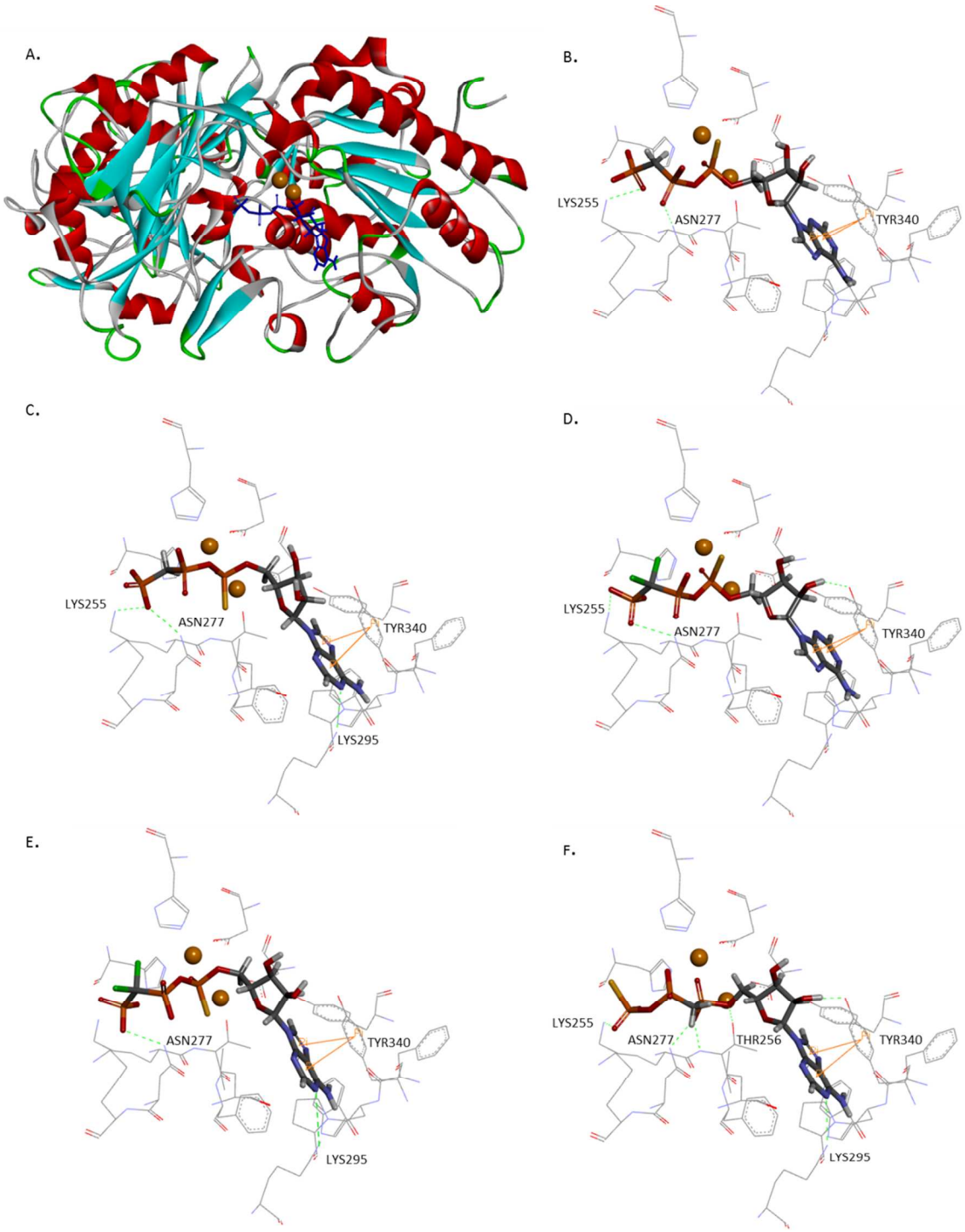
A.
B.
LYS255
ASN277
TYR340
C.
LYS255
ASN277
TYR340
LYS295
D.
LYS255
ASN277
TYR340
E.
ASN277
TYR340
LYS295
F.
LYS255
ASN277
THR256
TYR340
LYS295

Figure 8

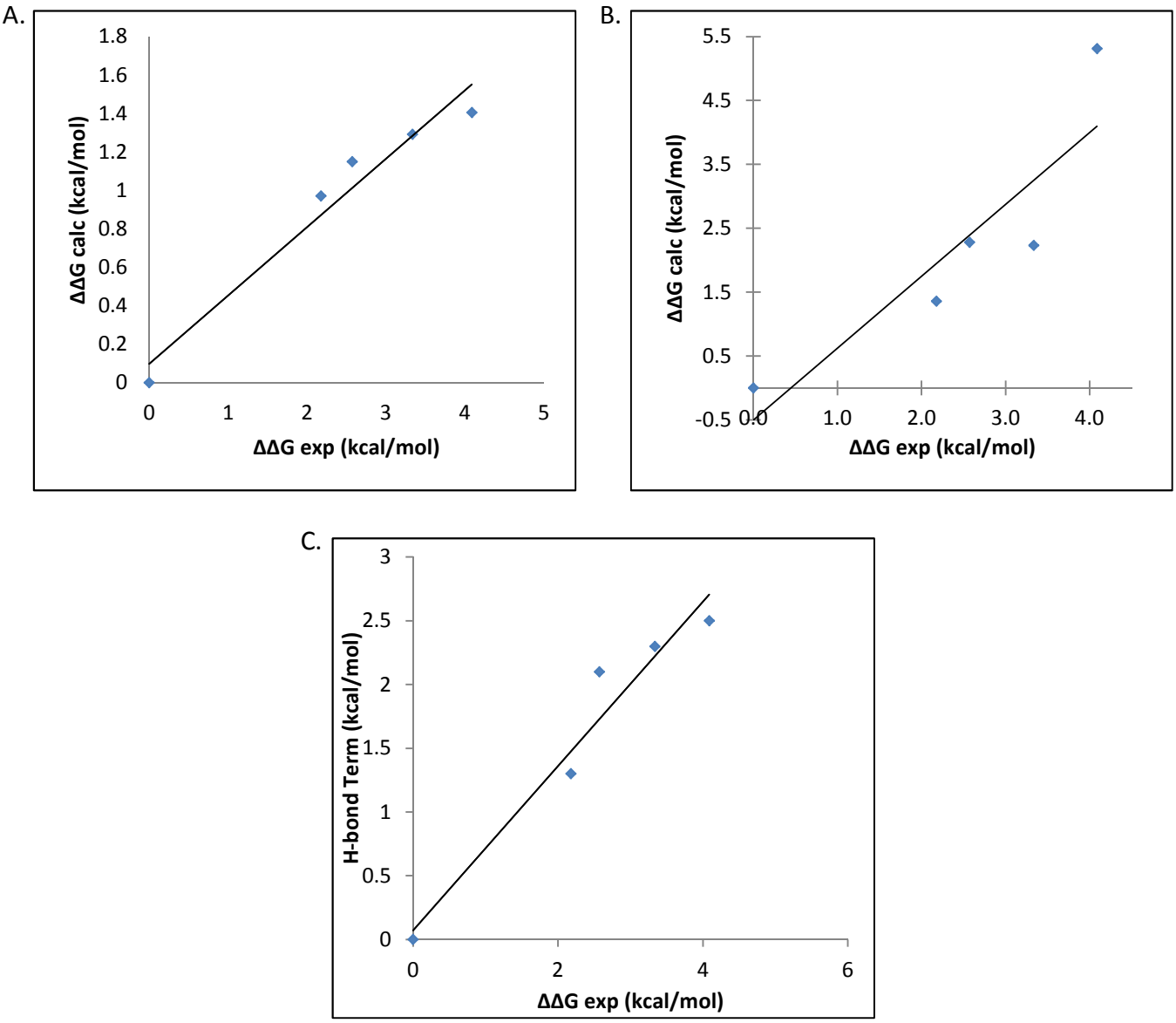
A.
ΔΔG calc (kcal/mol)
ΔΔG exp (kcal/mol)
B.
ΔΔG calc (kcal/mol)
ΔΔG exp (kcal/mol)
C.
H-bond Term (kcal/mol)
ΔΔG exp (kcal/mol)

Figure 9

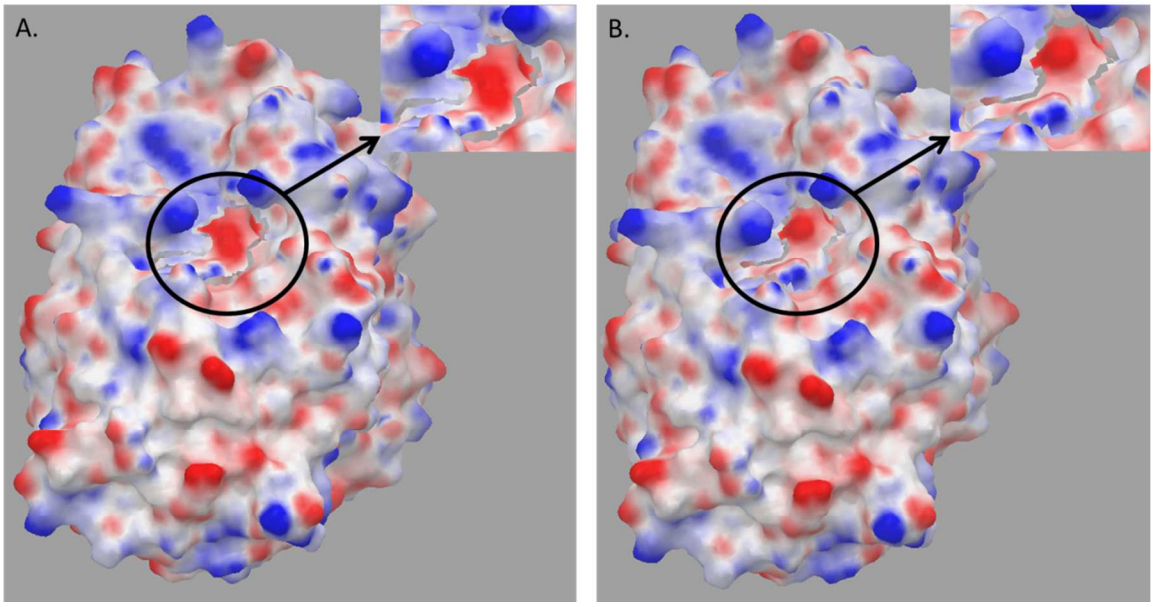

Schemes

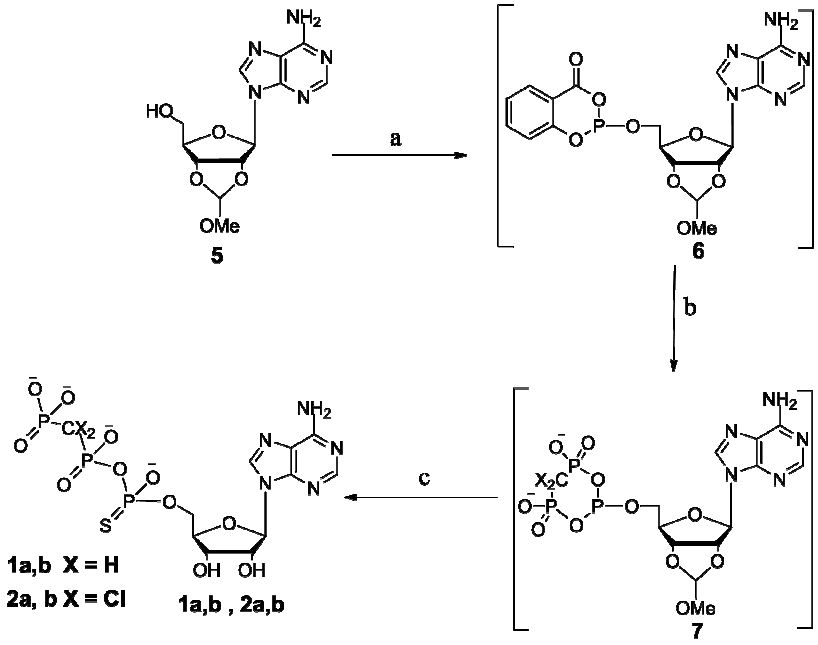

Scheme 1.

Reaction conditions: (a) 2-chloro-4H-1,3,2-benzodioxaphosphorin-4-one, DMF, pyridine, RT, 1h; (b) bis-(tetrabutylammonium)methylenediphosphonate or bis-(tetrabutylammonium)dichloromethylenediphosphonate, DMF, tributylamine, RT, 2 h; (c) 1. S_8, 0^0C, 1.5 h; 2. 1 M TEAB, 0.5 h, 3. 10% HCl, pH 2.5, 3 h, 4. 10% NH_4OH, pH 7, RT, 45 min. Analogues **1** and **2** were obtained in 9% and 17% yields, respectively. Compounds **6** and **7** are reaction intermediates and were not isolated,

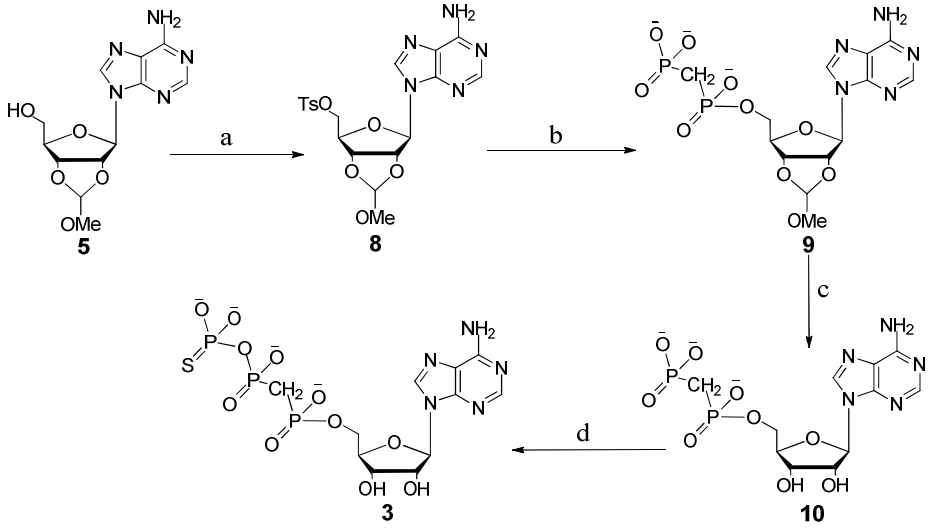

Scheme 2.

Reaction conditions: (a) TsCl, DMAP, DCM, RT, 3 h; (b) bis-(tetrabutylammonium)methylenediphosphonate, DMF, RT, 24 h (50% yield); (c) 1. 10% HCl, pH 2.5, RT, 3 h; 2. 10% NH_4OH, pH 7, RT, 45 min; (d) 1. CDI, DMF, RT, 5 h ; 2. $ZnCl_2$, MeOH, RT, 8 min; 3. tri-n-octylamine and tri-butylamine PSO_3^{3-}, RT, 3 h ; 4. EDTA, H_2O, RT, 10 min (29% yield).

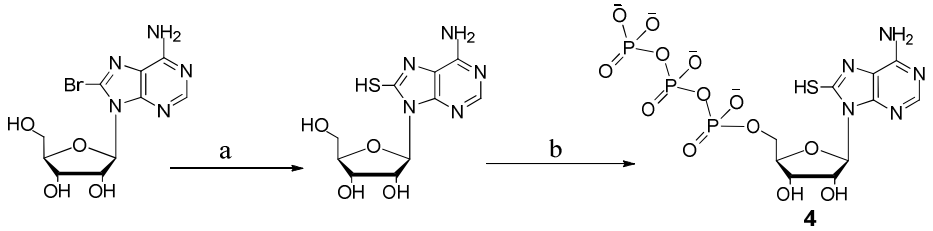

Scheme 3.

Reaction conditions: (a) NaSH, DMF 12 h; (b) 1. $POCl_3$, proton sponge, trimethylphosphate, -15^{0}C, 3 h; 2. pyrophosphate, DMF, 2 h (60% yield).

Tables

Table 1. Hydrolysis of analogues **1-4** by human ectonucleotidases

	relative activity (% ± SD of ATP hydrolysis)					
human ectonucleotidase	**1a**	**1b**	**2a**	**2b**	**3**	**4**
NTPDase1	4.4 ± 0.2	5.4 ± 0.2	5.3 ± 0.2	5.4 ± 0.2	5.3 ± 0.2	43 ± 2
NTPDase2	4.7 ± 1.7	5.5 ± 0.3	5.2 ± 0.1	5.5 ± 0.2	4.7 ± 0.2	73 ± 2
NTPDase3	4.2 ± 0.2	4.8 ± 0.2	5.2 ± 0.2	5.4 ± 0.2	4.8 ± 0.2	51 ± 3
NTPDase8	4.4 ± 0.2	5.3 ± 0.2	4.3 ± 0.1	5.3 ± 0.2	5.2 ± 0.2	73 ± 1
NPP1	ND	4 ± 0.8	ND	ND	ND	54 ± 2
NPP3	1.2 ± 0.9	4 ± 0.8	ND	ND	ND	32 ± 2

Adenosine triphosphate analogues **1-4** were incubated in the presence of the indicated ectonucleotidases at the concentration of 100 μM. The activity with 100 μM ATP was set as 100% which was 807 ± 35, 1051 ± 45, 240 ± 17 and 122 ± 7 [nmol Pi·min^{-1}·mg protein^{-1}] for NTPDase1, -2, -3 and -8, respectively. For NPP1 and NPP3, 100% of the activity with 100 μM ATP as the substrate was 67 ± 5 and 54 ± 2 [nmol of nucleotide·min^{-1}·mg protein^{-1}], respectively. Data presented are the means ± SD of results from 3 experiments carried out in triplicates. ND = no hydrolysis detected.

Table 2. Effect of analogues **1-3** on human NTPDase1, -2, -3, -8 activity.

Enzyme	1a	1b	2a	2b	3
	Inhibition [%] ± SD				
human NTPDase1	58.4 ± 2.1	0.5 ± 0.02	0.5 ± 0.01	21.6 ± 1.0	18.7 ± 0.8
human NTPDase2	16.3 ± 0.6	9.9 ± 0.4	11.2 ± 0.5	12.7 ± 0.5	15.4 ± 0.7
human NTPDase3	40.2 ± 2.0	18.7 ± 0.8	21.8 ± 1.0	24.0 ± 1.2	26.8 ± 1.1
human NTPDase8	7.0 ± 0.3	0.5 ± 0.01	4.9 ± 0.2	1.5 ± 0.06	0.50 ± 0.02

ATP was used as the substrate in the presence of either analogue **1a**, **1b**, **2a**, **2b** and **3**. Both substrate and analogues **1-3**, were studied at 100 μM. The 100% activity was set with the substrate ATP alone which was 807±35, 1051±45, 240±17, 122±7 and… [nmol $Pi \cdot min^{-1} \cdot mg\ protein^{-1}$] for NTPDase1, -2, -3 -8, and TNAP respectively. Data presented are the mean ± SD of 3 experiments carried out in triplicates.

Table 3. Kinetic parameters and IC_{50} of NPP1 inhibition

inhibitor	K_i [μM]	K_i' [μM]	IC_{50} [μM]
1a	4.5 ± 0.03	4.5 ± 0.003	16.3 ± 0.04
1b	1.3 ± 0.01	-71.5 ± 0.5	18.7 ± 0.03
2a	0.685 ± 0.005	-12.5 ± 0.1	0.6 ± 0.01
2b	15.2 ± 0.1	-192.0 ± 1	31.2 ± 0.1
3	0.02 ± 0.0001	-9.0 ± 0.05	0.39 ± 0.001

For K_i and K_i' determinations, pNP-TMP (substrate) and analogues **1-3** were used in the concentration range of $2.5 \cdot 10^{-5}$-$1 \cdot 10^{-3}$ M. For IC_{50} determinations, pNP-TMP concentration was $5 \cdot 10^{-5}$ M and inhibitors ranged from $5 \cdot 10^{-7}$ to $1 \cdot 10^{-3}$ M. All experiments were performed three times in triplicates.

Table 4. EC_{50} values for $[Ca^{2+}]_i$ elevation by analogues **1-3**, mediated by $P2Y_{1,11}$ -receptors

receptor subtype	nucleotide analogue	EC_{50} ± SEM (μM), $[Ca^{2+}]_i$ elevation	increase in efficacy [a] vs ATP
$P2Y_1$	**1a**	not active, n.r [c]	-
	1b	not active, slight response [b]	-
	2a	not active, n.r [c]	-
	2b	not active, n.r [c]	-
	3	not active, slight response [b]	-
	ATP [a]	0.85±0.047	1
$P2Y_{11}$	**1a**	not active, n.r. [c]	-
	1b	0.9±0.075	7.4
	2a	not active, n.r [c]	-
	2b	3.0±1.46	2.2
	3	1±0.49	6.7
	ATP [a]	6.7±0.87	1

[a] Efficacy is given as the EC_{50} value of the tested nucleotide in relation to the EC_{50} value of the endogenous agonist ATP. ATP was selected as the common reference agonist at both $P2Y_1$ and $P2Y_{11}$ receptors, although ADP is the preferred endogenous $P2Y_1$ receptor agonist.

[b] No response up to 1 μM; only 10 μM agonist concentration evoked response corresponding to 40% of maximal response of endogenous ligand ATP. For technical reasons, higher concentrations were not tested.

[c] Agonist showed no response up to 10 μM concentration

Table of Contents Graphics

Highly potent and selective nucleotide pyrophosphatase/phosphodiesterase I (NPP1) inhibitors based on an adenosine 5'-(α- or γ)-thio, (α,β- or β,γ)-methylene scaffold

Yael Nadel[a], Yocheved Gliad[a], Gal Ben-David[a], Hanoch Sendrowitz[a], Joanna Lecka[b], Jean Sévigny[b], Daniel Förster[c], Georg Reiser[c], Sarah Kenigsberg[a], Jean Camden[d], Gary A. Weisman[d], and Bilha Fischer*[a]

[a] Department of Chemistry, Bar-Ilan University, Ramat-Gan 52900 Israel,

[b] Centre de Recherche en Rhumatologie et Immunologie, Centre Hospitalier Universitaire de Québec, Université Laval, Québec, QC, Canada,

[c] Otto von Guericke University, Leipziger Str. 44, 39120, Magdeburg, Germany

[d] Biochemistry Department, 540E Bond Life Sciences Center, University of Missouri, Columbia, Missouri 65211

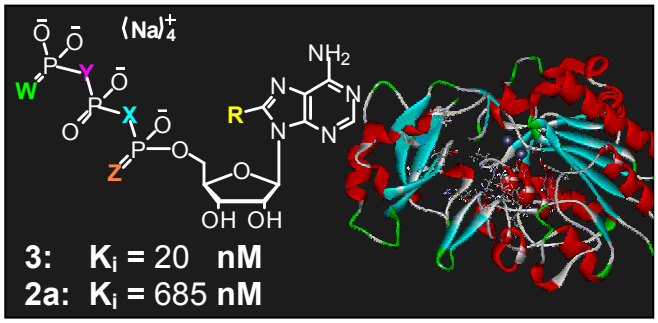

REFERENCES

(1) Kukulski, F.; Levesque, S. A.; Lavoie, E. G.; Lecka, J.; Bigonnesse, F.; Knowles, A. F.; Robson, S. C.; Kirley, T. L.; Sévigny, J. Comparative hydrolysis of P2 receptor agonists by NTPDases 1, 2, 3, and 8. *Purinerg. Signal.* **2005**, *1*, 193-204.

(2) Kukulski, F.; Lévesque, S. A.; Sévigny, J. Chapter 9 - Impact of Ectoenzymes on P2 and P1 Receptor Signaling. In *Adv. Pharmacol.*, Jacobson, K. A.; Linden, J., Eds. Academic Press: 2011; Vol. *Volume 61*, pp 263-299.

(3) Stefan, C.; Jansen, S.; Bollen, M. NPP-type ectophosphodiesterases: unity in diversity. *Trends Biochem. Sci.* **2005**, *30*, 542-550.

(4) Zimmermann, H.; Zebisch, M.; Sträter, N. Cellular function and molecular structure of ecto-nucleotidases. *Purinerg. Signal.* **2012**, *8*, 437-502.

(5) Gijsbers, R.; Ceulemans, H.; Stalmans, W.; Bollen, M. Structural and catalytic similarities between nucleotide pyrophosphatases/phosphodiesterases and alkaline phosphatases. *J. Biol. Chem.* **2001**, *276*, 1361-1368.

(6) Stefan, C.; Jansen, S.; Bollen, M. Modulation of purinergic signaling by NPP-type ectophosphodiesterases. *Purinerg. Signal.* **2006**, *2*, 361-370.

(7) Bollen, M.; Gijsbers, R.; Ceulemans, H.; Stalmans, W.; Stefan, C. Nucleotide pyrophosphatases/phosphodiesterases on the move. *Crit. Rev. Biochem. Mol.* **2000**, *35*, 393-432.

(8) Rosenthal, A. K.; Hempel, D.; Kurup, I. V.; Masuda, I.; Ryan, L. M. Purine receptors modulate chondrocyte extracellular inorganic pyrophosphate production. *Osteoarthr. Cartil.* **2010**, *18*, 1496-1501.

(9) Thouverey, C.; Bechkoff, G.; Pikula, S.; Buchet ,R. Inorganic pyrophosphate as a regulator of hydroxyapatite or calcium pyrophosphate dihydrate mineral deposition by matrix vesicles. *Osteoarthr. Cartil.* **2009**, *17*, 64-72.

(10) Ciancaglini, P.; Yadav, M. C.; Simão, A. M. S.; Narisawa, S.; Pizauro, J. M ;. Farquharson, C.; Hoylaerts, M. F.; Millán, J. L. Kinetic analysis of substrate utilization by native and TNAP-, NPP1-, or PHOSPHO1-deficient matrix vesicles. *J. Bone Miner. Res.* **2010**, *25*, 716-723.

(11) Derfus, B. A.; Kurtin, S. M.; Camacho, N. P.; Kurup ,I.; Ryan, L. M. Comparison of matrix vesicles derived from normal and osteoarthritic human articular cartilage. *Connect. Tissue Res.* **1996**, *35*, 337-342.

(12) Karpouzas, G. A.; Terkeltaub, R. A. New developments in the pathogenesis of articular cartilage calcification. *Curr. Rheumatol. Rep.* **1999**, *1*, 121-127.

(13) Maddux, B. A.; Sbraccia, P.; Kumakura, S.; Sasson, S.; Youngren, J.; Fisher, A.; Spencer, S.; Grupe, A.; Henzel, W.; Stewart, T. A.; et al. Membrane glycoprotein PC-1 and insulin resistance in non-insulin-dependent diabetes mellitus. *Nature* **1995**, *373*, 448-451.

(14) Grupe, A.; Alleman, J.; Goldfine, I. D.; Sadick, M.; Stewart, T. A. Inhibition of insulin receptor phosphorylation by PC-1 is not mediated by the hydrolysis of adenosine triphosphate or the generation of adenosine. *J. Biol. Chem.* **1995**, *270*, 22085-22088.

(15) Belfiore, A.; Costantino, A.; Frasca, F.; Pandini, G.; Mineo, R.; Vigneri, P.; Maddux, B.; Goldfine, I. D.; Vigneri, R. Overexpression of membrane glycoprotein PC-1 in MDA-MB231 breast cancer cells is associated with inhibition of insulin receptor tyrosine kinase activity. *J. Mol. Endocrinol.* **1996**, *10*, 1318-1326.

(16) Costanzo, B. V.; Trischitta, V.; Di Paola, R.; Spampinato, D.; Pizzuti, A.; Vigneri, R.; Frittitta, L. The Q allele variant (GLN121) of membrane glycoprotein PC-1 interacts with the insulin receptor and inhibits insulin signaling more effectively than the common K allele variant (LYS121). *Diabetes* **2001**, *50*, 831-836.
(17) Aerts, I.; Martin, J. J.; De Deyn, P. P.; Van Ginniken, C.; Van Ostade, X.; Kockx, M.; Dua, G.; Slegers, H. The expression of ecto-nucleotide pyrophosphatase/phosphodiesterase 1 (E-NPP1) is correlated with astrocytic tumor grade. *Clin. Neurol. Neurosurg.* **2011**, *113*, 224-229.
(18) Grobben, B.; Anciaux, K ;.Roymans, D.; Stefan, C.; Bollen, M.; Esmans, E. L.; Slegers, H. An ecto-nucleotide pyrophosphatase is one of the main enzymes involved in the extracellular metabolism of ATP in rat C6 glioma. *J. Neurochem.* **1999**, *72*, 826-834.
(19) Patel, S. D.; Habeski ,W. M.; Cheng, A. C.; de la Cruz, E.; Loh, C.; Kablaoui, N. M. Quinazolin-4-piperidin-4-methyl sulfamide PC-1 inhibitors: Alleviating hERG interactions through structure based design. *Bioorg. Med. Chem. Let.* **2009**, *19*, 3339-3343.
(20) Khan, K. M.; Fatima, N ;.Rasheed, M.; Jalil, S.; Ambreen, N.; Perveen, S.; Choudhary, M. I. 1,3,4-Oxadiazole-2(3H)-thione and its analogues: A new class of non-competitive nucleotide pyrophosphatases/phosphodiesterases 1 inhibitors. *Bioorg. Med. Chem.* **2009**, *17*, 7816-7822.
(21) Eliahu, S.; Lecka, J.; Reiser, G.; Haas, M.; Bigonnesse, F.; Levesque, S. A.; Pelletier, J.; Sévigny, J.; Fischer, B. Diadenosine 5 ',5 "-(Boranated)polyphosphonate Analogues as Selective Nucleotide Pyrophosphatase/Phosphodiesterase Inhibitors. *J. Med .Chem.* **2010**, *53*, 8485-8497.
(22) Lecka, J.; Ben-David, G.; Simhaev, L.; Eliahu, S.; Oscar, J.; Luyindula, P.; Pelletier, J.; Fischer, B.; Senderowitz, H.; Sévigny, J. Nonhydrolyzable ATP Analogues as Selective Inhibitors of Human NPP1: A Combined Computational/Experimental Study. *J. Med. Chem.* **2013**, *56*, 8308-8320.
(23) Bobyr, E.; Lassila, J. K.; Wiersma-Koch, H. I.; Fenn, T. D.; Lee, J. J.; Nikolic-Hughes, I.; Hodgson, K. O.; Rees, D. C.; Hedman, B.; Herschlag, D. High-resolution analysis of Zn(2+) coordination in the alkaline phosphatase superfamily by EXAFS and x-ray crystallography. *J. Mol. Biol.* **2012**, *415*, 102-117.
(24) Asensio, A. C.; Rodríguez-Ferrer, C. R.; Castañeyra-Perdomo, A.; Oaknin, S.; Rotllán, P. Biochemical analysis of ecto-nucleotide pyrophosphatase phosphodiesterase activity in brain membranes indicates involvement of NPP1 isoenzyme in extracellular hydrolysis of diadenosine polyphosphates in central nervous system. *Neurochem. Int.* **2007**, *50*, 581-590.
(25) Wojcik, M.; Stec, W. The effect of divalent cations on the catalytic activity of the human plasma 3′-exonuclease. *BioMetals* **2010**, *23*, 1113-1121.
(26) Lippard, S. J.; Berg, J. *Univeristy Science Books: Mill Vally*. 1994; p 21-22.
(27) Major, D. T.; Fischer, B. Molecular Recognition in Purinergic Receptors. 1. A Comprehensive Computational Study of the h-P2Y1-Receptor. *J. Med. Chem.* **2004**, *47*, 4391-4404.
(28) Liang, F.; Jain, N.; Hutchens, T.; Shock, D. D.; Beard, W. A.; Wilson, S. H.; Chiarelli, M. P.; Cho, B. P. α,β-Methylene-2'-deoxynucleoside 5'-Triphosphates as Noncleavable Substrates for DNA Polymerases: Isolation, Characterization, and Stability

Studies of Novel 2'-Deoxycyclonucleosides, 3,5'-Cyclo-dG, and 2,5'-Cyclo-dT. *J. Med. Chem.* **2008**, *51*, 6460-6470.
(29) Halbfinger, E.; Major, D .T.; Ritzmann, M.; Ubl, J.; Reiser, G.; Boyer, J. L.; Harden, K. T.; Fischer, B. Molecular Recognition of Modified Adenine Nucleotides by the P2Y1-Receptor. 1. A Synthetic, Biochemical, and NMR Approach. *J. Med. Chem.* **1999**, *42*, 5325-5337.
(30) Jacobson ,K. A.; Ivanov, A. A.; de Castro, S.; Harden, T. K.; Ko, H. Development of selective agonists and antagonists of P2Y receptors. *Purinerg. Signal.* **2009**, *5*, 75-89.
(31) Cornish-Bowden, A. A simple graphical method for determining the inhibition constants of mixed, uncompetitive and non-competitive inhibitors. *Biochem. J.* **1974**, *137*, 143-150.
(32) Dixon, M. The effect of pH on the affinities of enzymes for substrates and inhibitors. *Biochem. J.* **1953**, *55*, 161-170.
(33) Erlinge, D. P2Y receptors in health and disease. *Adv. Pharmacol.* **2011**, *61*, 417-439.
(34) Hoebertz, A.; Mahendran, S.; Burnstock, G.; Arnett, T. R. ATP and UTP at low concentrations strongly inhibit bone formation by osteoblasts: a novel role for the P2Y2 receptor in bone remodeling. *J. Cell. Biochem.* **2002**, *86*, 413-419.
(35) Gallagher, J. A.; Buckley, K. A. Expression and function of P2 receptors in bone. *J. Musculoskeletal Neuronal Interact.* **2002**, *2*, 432-439.
(36) Parr, C. E.; Sullivan, D. M.; Paradiso, A. M.; Lazarowski, E. R.; Burch, L. H.; Olsen, J. C.; Erb, L.; Weisman, G. A.; Boucher, R. C.; Turner, J. T. Cloning and expression of a human P2U nucleotide receptor, a target for cystic fibrosis pharmacotherapy. *Proc. Natl. Acad. Sci. U. S. A.* **1994**, *91*, 3275-3279.
(37) Labotka, R. J.; Omachi, A .The pH dependence of red cell membrane transport of titratable anions studied by NMR spectroscopy. *Journal of Biological Chemistry* **1988**, *263*, 1166-1173.
(38) Blackburn, G. M.; Kent, D. E.; Kolkmann, F. Three new [small beta],[gamma]-methylene analogues of adenosine triphosphate. *J. Chem. Soc. Chem. Comm.* **1981**, 1188-1190.
(39) Wang, G.; Boyle, N.; Chen, F.; Rajappan, V.; Fagan, P.; Brooks, J. L.; Hurd, T.; Leeds, J. M.; Rajwanshi, V. K.; Jin, Y.; Prhavc, M.; Bruice, T. W.; Cook, P. D. Synthesis of AZT 5-'Triphosphate Mimics and Their Inhibitory Effects on HIV-1 Reverse Transcriptase. *J. Med. Chem.* **2004**, *47*, 6902-6913.
(40) Jacobson, K.; Balasubramanian, R.; Deflorian, F.; Gao, Z.-G. G protein-coupled adenosine (P1) and P2Y receptors: ligand design and receptor interactions. *Purinerg. Signal.* **2012**, *8*, 419-436.
(41) Jacobson, K. A.; Boeynaems, J.-M. P2Y nucleotide receptors: promise of therapeutic applications. *Drug Discov. Today* **2010**, *15*, 570-578.
(42) Van der Weyden, L.; Adams, D. J.; Luttrell, B. M.; Conigrave, A. D.; Morris, M. B. Pharmacological characterisation of the P2Y(11) receptor in stably transfected haematological cell lines. *Mol. Cell. Biochem.* **2000**, *213*, 75-81.
(43) Van der Weyden, L.; Rakyan, V.; Luttrell, B. M.; Morris, M. B.; Conigrave, A .D. Extracellular ATP couples to cAMP generation and granulocytic differentiation in human NB4 promyelocytic leukaemia cells. *Immunol. Cell Biol.* **2000**, *78*, 467-473.

(44) Eliahu, S. E.; Camden, J.; Lecka, J.; Weisman, G. A.; Sévigny, J.; Gelinas, S.; Fischer, B. Identification of hydrolytically stable and selective P2Y1 receptor agonists. *Eur. J. Med. Chem.* **2009**, *44*, 1525-1536.
(45) Houston, D.; Costanzi, S.; Jacobson, K. A.; Harden, T. K. Development of selective high affinity antagonists, agonists, and radioligands for the P2Y(1) receptor. *Comb. Chem. High Throughput Screen.* **2008**, *11*, 410-419.
(46) Zylberg, J.; Ecke, D.; Fischer, B.; Reiser, G. Structure and ligand-binding site characteristics of the human P2Y11 nucleotide receptor deduced from computational modelling and mutational analysis. *J. Biochem.* **2007**, *405*, 277-286.
(47) Ecke, D.; Tulapurkar, M. E.; Nahum, V.; Fischer, B.; Reiser, G. Opposite diastereoselective activation of P2Y1 and P2Y11 nucleotide receptors by adenosine 5'-O-(α-boranotriphosphate) analogues. *Br. J. Pharmacol.* **2006**, *149*, 416-423.
(48) Haas, M.; Ben-Moshe, I.; Fischer, B.; Reiser, G. Sp-2-propylthio-ATP-α-B and Sp-2-propylthio-ATP-α-B,β-γ-dichloromethylene are novel potent and specific agonists of the human P2Y11 receptor. *Biochem. Pharmacol.* **2013**, *86*, 645-655.
(49) Ecke, D.; Hanck, T.; Tulapurkar, M. E.; Schaefer, R.; Kassack, M.; Stricker, R.; Reiser, G. Hetero-oligomerization of the P2Y11 receptor with the P2Y1 receptor controls the internalization and ligand selectivity of the P2Y11 receptor. *Biochem. J.* **2008**, *409*, 107-116.
(50) Hoffmann, C.; Moro, S.; Nicholas, R. A.; Harden, T. K.; Jacobson, K. A. The role of amino acids in extracellular loops of the human P2Y1 receptor in surface expression and activation processes. *J Biol Chem* **1999**, *274*, 14639-14647.
(51) Communi, D.; Govaerts, C.; Parmentier, M.; Boeynaems, J. M. Cloning of a human purinergic P2Y receptor coupled to phospholipase C and adenylyl cyclase. *J Biol Chem* **1997**, *272*, 31969-31973.
(52) Costanzi, S.; Mamedova, L ;.Gao, Z. G.; Jacobson, K. A. Architecture of P2Y nucleotide receptors: structural comparison based on sequence analysis, mutagenesis, and homology modeling. *J. Med. Chem.* **2004**, *47*, 5393-5404.
(53) Burnstock, G. Purinergic signalling: past, present and future. *Braz. J. Med. Biol. Res.* **2009**, *42*, 3-8.
(54) Accurso, F. J.; Moss, R. B.; Wilmott, R. W.; Anbar, R. D.; Schaberg, A. E.; Durham, T. A.; Ramsey, B. W. Denufosol Tetrasodium in Patients with Cystic Fibrosis and Normal to Mildly Impaired Lung Function *.Am. J. Respir. Crit. Care. Med.* **2011**, *183*, 627-634.
(55) De Clercq, E. A 40-Year Journey in Search of Selective Antiviral Chemotherapy. *Annu. Rev. Pharmacol. Toxicol.* **2011**, *51*, 1-24.
(56) Gendron, F. P.; Halbfinger, E.; Fischer, B.; Duval, M.; D'Orleans-Juste, P.; Beaudoin, A. R. Novel inhibitors of nucleoside triphosphate diphosphohydrolases: Chemical synthesis and biochemical and pharmacological characterizations. *J. Med. Chem.* **2000**, *43*, 2239-2247.
(57) Kaczmarek, E.; Koziak, K.; Sévigny, J.; Siegel, J .B.; Anrather, J.; Beaudoin, A. R.; Bach, F. H.; Robson, S. C. Identification and characterization of CD39/vascular ATP diphosphohydrolase. *J. Biol. Chem.* **1996**, *271*, 33116-33122.
(58) Knowles, A. F.; Chiang, W. C. Enzymatic and transcriptional regulation of human ecto-ATPase/E-NTPDase 2. *Arch. Biochem. Biophys.* **2003**, *418*, 217-27.

(59) Smith, T. M.; Kirley, T. L. Cloning, sequencing, and expression of a human brain ecto-apyrase related to both the ecto-ATPases and CD39 ecto-apyrases1. *Biochim. Biophys. Acta.* **1998**, *1386*, 65-78.
(60) Fausther, M.; Lecka, J.; Kukulski, F.; Levesque, S. A.; Pelletier, J.; Zimmermann, H.; Dranoff, J. A.; Sévigny, J. Cloning, purification, and identification of the liver canalicular ecto-ATPase as NTPDase8. *Am. J. Physiol. Gastrointest. Liver Physiol.* **2007**, *292*, G785-95.
(61) Belli, S. I.; Goding, J. W. Biochemical characterization of human PC-1, an enzyme possessing alkaline phosphodiesterase I and nucleotide pyrophosphatase activities. *Eur. J. Biochem.* **1994**, *226*, 433-43.
(62) Jin-Hua, P.; Goding, J. W.; Nakamura, H.; Sano, K. Molecular cloning and chromosomal localization of PD-Ibeta (PDNP3), a new member of the human phosphodiesterase I genes. *Genomics* **1997**, *45*, 412-5.
(63) Lavoie, E. G.; Kukulski, F.; Levesque, S. A.; Lecka ,J.; Sévigny, J. Cloning and characterization of mouse nucleoside triphosphate diphosphohydrolase-3. *Biochem. Pharmacol.* **2004**, *67*, 1917-1926.
(64) Bradford, M. M. A rapid and sensitive method for the quantitation of microgram quantities of protein utilizing the principle of protein-dye binding. *Anal. Biochem.* **1976**, *72*, 248-254.
(65) Baikov, A. A.; Evtushenko, O. A.; Avaeva, S. M. A malachite green procedure for orthophosphate determination and its use in alkaline phosphatase-based enzyme immunoassay. *Anal. Biochem.* **1988**, *171*, 266-270.
(66) Ubl, J. J.; Vohringer, C.; Reiser, G. Co-existence of two types of $[Ca^{2+}]_i$-inducing protease-activated receptors (PAR-1 and PAR-2) in rat astrocytes and C6 glioma cells. *Neuroscience* **1998**, *86*, 597-609.
(67) Tulapurkar ,M. E.; Laubinger, W.; Nahum, V.; Fischer, B.; Reiser, G. Subtype specific internalization of P2Y1 and P2Y2 receptors induced by novel adenosine 5'-O-(1-boranotriphosphate) derivatives. *Br. J. Pharmacol.* **2004**, *142*, 869-878.
(68) Tulapurkar, M. E.; Zundorf ,G.; Reiser, G. Internalization and desensitization of a green fluorescent protein-tagged P2Y nucleotide receptor are differently controlled by inhibition of calmodulin-dependent protein kinase II. *J. Neurochem.* **2006**, *96*, 624-634.
(69) Accelrys, S. I. *Discovery Studio Modeling Environment*, San Diego, 2010.
(70) Friesner, R. A.; Banks, J. L.; Murphy, R. B.; Halgren, T. A.; Klicic, J. J.; Mainz, D. T.; Repasky, M. P.; Knoll, E. H.; Shelley, M.; Perry, J. K.; Shaw, D. E.; Francis, P.; Shenkin, P. S. Glide :a new approach for rapid, accurate docking and scoring. 1. Method and assessment of docking accuracy. *J. Med. Chem.* **2004**, *47*, 1739-1749.
(71) Schrödinger. *Glide*, Schrodinger, Inc. : New York, NY, 2009.
(72) Schrödinger. *Maestro*, Schrodinger, LLC: New York, NY, 2009.
(73) Friesner, R. A.; Murphy, R. B.; Repasky, M. P.; Frye, L. L.; Greenwood, J. R.; Halgren, T. A.; Sanschagrin, P. C.; Mainz, D. T. Extra precision glide: docking and scoring incorporating a model of hydrophobic enclosure for protein-ligand complexes. *J. Med. Chem.* **2006**, *49*, 6177-6196.